Repeated blood-brain barrier opening using low-intensity pulsed ultrasound mitigates amyloid pathology

Michael Canney[1], Guillaume Bouchoux[1], Alexandre Carpentier[2], Pierre De Rossi[1*]

[1]Carthera, Lyon, France

[2]Sorbonne Université, AP-HP, Hôpitaux Universitaires La Pitié Salpêtrière - Charles Foix, Service de Neurochirurgie, Paris, France

*corresponding author: pierre.derossi@carthera.eu

Abstract

Background: The delivery of large molecules to the pathological brain is one of the main obstacles in the development of disease-modifying drugs. This is partly due to the presence of the blood-brain barrier (BBB), which blocks the free passage of lipophobic molecules and those larger than 400 Da. One strategy to bypass this natural barrier is to use low intensity pulsed ultrasound (LIPU) to oscillate circulating micro-sized microbubbles which then exert mechanical stress on the vessel walls. This procedure allows for temporary disruption of the BBB and enhanced local delivery of therapeutics from the blood to the brain parenchyma. In this study, the effect of repeated BBB opening on neuroinflammation in a healthy mouse model was first explored followed by the effect of repeated opening on amyloid pathology in a model for Alzheimer's disease.

Methods: A cohort of wildtype mice was used to determine the effect of a single BBB opening mediated by ultrasound/microbubbles (US/MB) on the inflammatory profile, using RT-Q-PCR on brain extracts at 2-, 4-, 8- and 15-days post opening. A second cohort of ARTE10 mice, a mouse model for amyloid pathology, was treated with a different sequence of repeated US/MB mediated BBB opening to explore the effect on the pathology. Tissues were also analyzed for immune cell infiltration, microglia and astrocyte activation, and inflammatory response.

Results: Our results demonstrate that the opening of the BBB leads to a mild inflammatory response in wild-type animals. However, repeated opening of the BBB in the ARTE10 model resulted in a decrease in amyloid pathology, along with a mild increase of growth factor.

Conclusions: Altogether, this study suggests that sonication is not only a safe method to deliver therapeutics to the brain but could also have synergistic effects in the treatment of neurodegenerative diseases.

Introduction

Alzheimer's disease (AD) is a neurodegenerative disorder that slowly affects memory, thinking and behavior, associated with progressive neurodegeneration. AD is characterized by two molecular hallmarks: the extracellular aggregation of amyloid-beta in plaques and the intracellular aggregation of hyperphosphorylated tau, resulting in tau tangles. These progressive pathological features have been hypothesized to lead to the resulting cognitive deterioration observed in patients.

While the last two decades of research have uncovered several risk factors for AD and led to the discovery of new pathways that may be responsible for disease onset, most pharmaceutical development has been focused on developing therapies targeting tau and amyloid. The hypothesis behind this strategy is that the removal of these pathological aggregates will lead to restoration of normal neuronal function and delay or stop the progression of the disease.

Recently, the first regulatory approvals have been obtained for antibody-based therapies targeting amyloid for the treatment of AD, despite only showing modest results in Phase 3 clinical trials[1]. However, one of the main obstacles that limit the efficacy of these antibody treatments targeting amyloid is the difficulty in bypassing the blood-brain barrier (BBB). Normally, only 0.01%[2] of the administered antibody reaches the brain. If higher parenchymal concentrations could be reached, we could observe a better clearance of the plaques associated with a better efficacy of these treatments, as recently demonstrated by the last results for the phase 2 clinical trial for the Trontinemab[3].

To overcome the BBB, ultrasound (US) technology can be used to temporarily disrupt the BBB and increase delivery of therapeutics. This method uses the combination of circulating/oscillating microbubbles (MB) administered intravenously and stimulated by low intensity pulsed ultrasound (LIPU) to disrupt the tight junctions of the BBB, allowing enhanced entry of molecules, ranging from small molecule therapeutics to large antibodies into the parenchyma[4–21]. This strategy has been used to enhance delivery of therapeutics into the CNS of mouse models for AD[4,7,9]. In addition, a recent clinical trial by Rezai et al. 2024[15] has shown promising results for delivering the FDA-approved anti-amyloid therapy aducanumab in Alzheimer's patients using US/MB with a clinical ultrasound system. A 32% reduction in SUVR on ^{18}F-florbetaben PET scans was observed after 26 weeks in the regions that received treatment to open the BBB. These clinical results demonstrate the potential efficacy gained by the delivery of antibody therapies using ultrasound.

US-mediated BBB opening alone, without concomitant drug administration has also been shown to have beneficial effects, potentially by altering the immune microenvironment in Alzheimer's mouse models and in patients[4,22–30], with improved outcomes when coupled to anti-amyloid therapies[4,31–35]. Moreover, it was shown that opening of the BBB can also potentiate a diverse range beneficial biological effects including neurogenesis[36–38]. In amyloid models of the disease, repeated BBB opening decreased the number of amyloid deposits in the brain[22,24,27–30,35] and improved cognition[22,24,27,30]. Similarly, in tau models of the disease, repeated BBB opening was able to decrease tau pathology[39,40] and improve cognition[39]. Finally, in patients with AD, repeated opening of the BBB using US was shown to be safe[41–44] and efficient to mitigate the amyloid burden in the brain[43,44].

While several studies have already explored the effect of BBB opening using US/MB on the inflammatory profile of the brain at short term, evidence is still lacking on the lasting effects of BBB opening in the healthy brain as well as its potential as a therapeutic approach for neurodegenerative diseases. In this preliminary study, we explored the effect of BBB opening in wildtype mice and in a mouse model for amyloid pathology (ARTE10) on the inflammatory profile of the brain and its effect on neuropathological hallmarks.

Results

Unique BBB disruption changes the molecular inflammatory signaling profile for several days

To better understand the effects of mechanical opening of the BBB by US/MB, we investigated blood-based markers and inflammatory markers following a single session of ultrasound to disrupt the BBB (experimental plan, Fig1A).

No significant changes in body weight or on the blood cell count were observed (Fig S1A, Fig1B-C). The only recorded change was a slight increase in the red blood cell count 15 days post opening. We used the S100b marker to monitor the opening of the BBB post procedure and its level overtime. As expected, we observed a drop of the S100b level over time reaching the lowest level 8 days after BBB opening (Fig S1B, measured by ELISA).

Once the safety of BBB opening was established, we performed RT-Q-PCR to explore the level of different inflammatory markers in the brain at several time points [2-, 4-, 8- and 15-days post opening] post BBB opening. Interestingly, the only significant increase compared to controls without BBB opening was an increase in *Il-6* mRNA levels, consistently over all timepoints. It is important to note that *Il-6* increase was correlated with an increase of red blood cells (Fig 1B)[45]. Notably, all the other factors measured were decreased, either transiently, or with a prolonged effect, up to 15 days post treatment.

Inflammatory chemokines *Cxcl1* and *Ccl2* as well as inflammatory cytokines *Il-1b*, *Il-10* and *Tnf-a* were decreased. While most of the chemokines decreased over 15 days post treatment, *Tnf-a* was only decreased in the first 48h of the protocol, with a recovery to baseline by day 4. Adhesion molecules *Icam1* and *E-selectin* were also decreased, with a recovery of *E-selectin* by day 15. The growth factors *Tgfb* and *Bdnf* were found to be significantly reduced after a single sonication. Finally, the transcription factor *Nfkb* was significantly decreased post sonication. Altogether, these results suggested that the opening of the BBB with the selected parameters did not lead to a pro-inflammatory response, or any significant changes to other physiological metrics in a healthy mouse model.

Different schedules of repeated BBB opening did not impact physiological output

Next, the effect of different sonication protocols was explored in a mouse model for AD that develops amyloid deposition (ARTE10). We tested different regimens of US/MB mediated BBB opening going from twice a week to once a month with sacrifice and profiling of different markers at one week or one month after the last sonication (Fig.2A). We first investigated the effect of repeated sonication on the general health and survival of the mice. We did not

observe major differences between groups (Fig. 2B). A few mice had weight reduction following the first session of the sonication but recovered in the following week(s).

Overall, our data suggests that LIPU-mediated BBB opening is a safe procedure that allows repetitive treatment. As performed for the WT cohort, the serum level of S100b was measured at different timepoints and postmortem (Fig 2CD). Our results did not show cumulative increases in this biomarker over the course of the treatment. This suggested that the BBB was able to restore itself between each session, leading to an apparent constant level of S100b in the blood. Altogether, these data demonstrated the low level of toxicity of a repeated protocol of sonication, as well as the structural plasticity of the BBB allowing repeated mechanical disruption of its structure.

Sonication frequency does not trigger inflammation in the brain over time

Using the post-mortem tissues from the ARTE10 cohort, we then investigated the effect of repeated BBB opening on inflammatory markers of the brain at the cellular and the molecular level. CD3, GFAP and Iba1 markers were used to explore T-cell infiltration, gliosis and microglial activation respectively (Fig. 3A). We used an automated pipeline of analysis, able to recognize the cells/markers of interest to extract the number of cells per mm^2 or the percentage of occupancy (see Supp Fig2. A-C showing the quantification mask for the 3 markers). The obtained results showed that repeated sonication did not lead to an increase of CD3+ cell infiltration (Fig3B and C). Only mild increase in astrogliosis was observed between Group 1 and Group 3 (Fig3D and F), as previously reported[46] and consistent with the level of S100b observed. In all the other conditions, as well as for all the conditions for Iba1, no difference between groups was detected (Fig3D-F). A few CD3+ cells were observed in the vicinity of amyloid deposits. As expected, GFAP+ and Iba+ cells tend to accumulate around the amyloid deposits. However, to explore how sonication stimulates the relocalization of inflammatory cells around the pathological aggregates, triggering their elimination, more in-depth studies will be required, to explore the cellular mechanisms triggered by the LIPU-mediated BBB opening.

We generated preliminary results on the mRNA expression of few inflammatory markers (as explored in Fig. 1). Interestingly, our results showed a decrease in the proinflammatory cytokines in all conditions, as was observed in wildtype mice (Fig. 1). Opposite to what was observed in the single BBB opening protocol, repeated opening of the BBB was associated with an increase of *bdnf* in most treatments (Supp fig 2D). This brings the possibility that the repeated mechanical opening of the BBB could favor the local release of growth factors, as it was observed in other studies[36–38].These data would require further investigation, but they provide an interesting first look at the molecular changes occurring during a repeated sonication regimen, which could provide additional benefits for the patients.

Monthly repeated sonication shows promising results on pathological hallmarks

Finally, we assessed the effect of repeated sonication on amyloid deposits in the ARTE10 model (Fig4A). The ARTE10 mouse model is characterized by the presence of amyloid and mineralized deposits in the brain (Supp fig 4A), a noticeable loss of hippocampal neurons (Suppl Fig4B), and the presence of amyloid deposition around the brain vasculature (Suppl Fig3C). Consistently across all analyses, our data showed a significant reduction of the amyloid load in the very sparse sonication regimen (Group 6), consisting of a monthly

sonication, compared to the other sonication regimens (Group 3 and 4), with more regular sonication regimen. While not significant, it is worth noting that Group 6 also showed a slight reduction in the amyloid load compared to the non-sonicated control (Group1). Indeed, if analyzed separately, the average size of amyloid deposits was significantly reduced, while the percentage of amyloid positive area showed a tendency to decrease under the monthly sonication regimen (Supp Fig4D). The treatment did not have any effect on the overall number of deposits. Taken together, these data confirm the results previously shown that ultrasound alone can have beneficial effects in the treatment of Alzheimer's pathology.

Discussion

Altogether, this short preliminary study showed that LIPU is a safe method to open the BBB, allowing repeated use with potential benefits in a pathological context. We previously demonstrated in a small cohort of nine patients with mild AD that seven repeated, bi-monthly LIPU-mediated BBB opening reduced the amyloid burden by 6.6% in the brain region targeted by the implantable ultrasound system used in the study[44]. The results from this preclinical study are in agreement and point to a modest effect of ultrasound alone on amyloid pathology. In depth analyses of the different types of amyloid aggregates showed that repeated sonication triggers a reduction in the amyloid deposit size and amyloid coverage in the brain. These results are encouraging and point out the potential for ultrasound-mediated BBB opening as a therapeutic tool by itself. Further research should focus on finding the best synergistic effects between a specific therapeutic compound and an optimized sonication regimen to improve the outcome for the patients.

Several studies have already explored the effect of sonication on amyloid pathology in AD models (see tables 4 and 5). However, the experimental designs between these different studies, including this one, make it complicated to grasp the real value of sonication in this pathology. In comparison to these models, ARTE10 model presents an amyloid deposition at 3 months, synaptic loss at 3 months, and a cognitive impairment at 12 months[47]. This model presents similarities with the TgCRND8 models. However, in the previously published studies, the animals were treated at a younger age (4.5mo in Jordao et al, 2010, 4mo in Jordao et al 2013, 6 to 8 mo in Burgess et al, 2014a and b, 7 mo in Poon et al, 2018). Our study explored the effect of repeated sonication in 1yo mice, where the amyloid deposition is already highly established and with a heavy load of amyloid deposits. 3TG and APP/PS1dE9 models were used at later stages, but the rate of amyloid deposition appears slower than in the ARTE10 mouse model (8mo in Shen et al, 2020; 2.5mo, 1yo and 2yo in Noel et al, 2023 and 14mo in Karakatsani et al, 2023, 12 and 14 mo in Hsu et al, 2018 and 16, 24 and 30 mo in Sun et al, 2021). To focus on comparable studies, we will only consider studies which used repeated sonication protocol to show the effect on the amyloid pathology[22,24,27–30,35]. Despite these experimental differences, similar effects were recorded, including our study: 1) Repeated sonication consistently triggers a decrease in the amyloid load across all models[22,24,27–30,35]; 2) A significant improvement of the cognitive performances[22,24,27,30], 3) An increased microglial activity around the deposits[22,29].

Our study demonstrated that in both a wildtype and a mouse model for AD with amyloid pathology (ARTE10), repeated LIPU-mediated BBB opening does not affect the general physiology of the mouse. However, we observed that a single sonication led to an increase of *Il-6*, while most of the other factors were either unchanged or slightly decreased (Fig.1D).

Il-6 is classically described as a pro-inflammatory cytokine with several key functions in the central nervous system but also shows anti-inflammatory functions in specific contexts[48]. *Il-6* has been shown to play a major role in activating microglia and favoring microvasculature repair after injury[49]. In brain diseases, *Il-6* expression was found to be increased in traumatic brain injury (TBI) as well as some initial steps of Alzheimer's disease[50–52], however with conflicting associated functions. While the increase of *Il-6* levels after TBI was associated with anti-inflammatory and pro-survival effects, sustained elevated levels of *Il-6* were shown to be detrimental by increasing neuronal excitability leading to potential seizures[48]. Moreover, *Il-6* stimulates angiogenesis following a stroke episode, highlighting its potent role in stimulating vasculature repair after vascular injuries[53]. In addition, *Il-6* is known to increase in response to tissue injuries and to induce hematopoiesis (increase in red blood cell, Fig1B)[45]. In our experiments, we hypothesized that the increase in *Il-6* was tightly correlated to the vasculature repair process, without triggering a pathological chronic inflammatory response. Indeed, other cytokines and chemokines were unchanged or decreased after BBB opening, pointing out the unique role of *Il-6* in this context.

Other factors like the *Tnf-a*, another known partner involved in pathogenesis of AD[54], showed a downregulation post BBB-opening. Interestingly, in the context of TBI, *Il-6* inhibits the production of *Tnf-a* as an anti-inflammatory process, as observed in our data[48]. *Tnf-a* plays a central role in neuroinflammation[55], which reinforces the observation that LIPU-mediated BBB opening does not trigger pathological inflammation. Similarly to *Tnf-a*, *Il-1b* is associated with a myriad of negative effects on the brain, in regard to seizures, a role in the development of different psychiatric disorders and neurodegenerative diseases[56–58]. More importantly for the BBB, the inhibition of the *Il-1b* pathway showed a positive effect on the brain vascularization[59]. Counter intuitively, we observed a decrease in level of *Il-10*, an anti-inflammatory cytokine of the brain, with important roles in the repair process of the brain[60] and limiting pathological inflammation[61]. This suggests that LIPU-mediated BBB-opening is not a major traumatic event in the brain and only triggers transient changes in inflammatory markers in the brain. Our results showed a transitory effect on astrocytic activation (Fig. 3F). These results are in accordance with recent publications, showing a transient activation of astrocytes and microglia in the first hours post sonication, with a normalization to baseline after few days[46,62–64].

In this direction, the decrease in *nfkb* expression confirms the minimal impact of our BBB opening strategy on neuroinflammation[65,66]. Similarly, Ccl2, a factor known for disrupting the BBB integrity[67–69], as well as favorizing the infiltration of leukocytes and monocytes to the brain parenchyma[67,70], was found decreased post sonication, reinforcing the idea that LIPU-mediated BBB opening is a mild disruption of the BBB itself, and does not trigger pathways observed in stroke- or infection-mediated BBB disruptions. Our study also showed a transient decrease in surface adhesion molecule expression *Icam* and *E-Selectin*. *E-Selectin* levels were recovered 8d post opening, while *Icam* took longer to recover. In a recent publication, it was shown that repeated sonication schedules could be favorable for the vasculature, by stimulating higher level of adhesion molecule VE-Cadherin [71]. To really understand the effect of repeated sonication on the vasculature, especially in the context of neurodegenerative diseases, more in-depth studies will be required in the future, using high spatial resolution techniques such as in vivo 2-photon microscopy and spatial transcriptomics and proteomics. These studies could bring evidence of the beneficial effect

of sonication in stimulating the repair process of the vasculature, and reperfusion of the brain[62].

Our study offers a unique timeline into the changes happening post BBB opening. Several studies attempted similar quantifications, however with a shorter timeline going up to 24h post sonication, versus 15 days in our study[72–74]. The data obtained 24h post sonication[72,73] showed a significant decrease in the magnitude of changes observed in the different factors, reaching similar amplitudes as what was observed in our study (0.5 to 1-fold change). Compared to these studies, our data showed that there are no negative long-term changes in induced neuroinflammation post sonication, confirming the normalizing level of all analyzed cytokines and chemokines in the previous studies. These results are a testimony to the transitory aspect of the US/MB-mediated BBB opening. It is however interesting to compare the data generated in our wildtype cohort, where a single BBB opening was performed, to the data obtained in our ARTE10 cohort, where different repeated sonication regimens were applied. Two main differences were observed between the two cohorts: The absence of *Il-6* increase and increase in *bdnf* expression in the repeated sonication cohort compared to the single sonication cohort. Increased *bdnf* was already observed post sonication[72] and suggested as the underlying mechanism responsible for stimulating neurogenesis in other studies[27,36–38]. For example, in Kovacs et al., *bdnf* levels were observed to increase around 24h post sonication. Our study showed that this increase might be transient, as we did not observe a detectable increase at 48h post-sonication or could be an effect of the much stronger sonication parameters used to disrupt the BBB in the Kovacs et al. study. However, as we observed an increase of *bdnf* levels after repeated sonication, it suggests that regular opening of the BBB could allow sustained levels of BDNF overtime, which could in turn have a beneficial effect, potentially through increased neurogenesis or higher neuronal excitability and synaptic homeostasis[75]. However, as observed for group 3 and 4, higher level of BDNF did not correlated with decrease of amyloid pathology. It is now well documented that neuronal activity correlates with amyloid beta secretion in the intercellular spaces[76–78]. These results would suggest that LIPU-mediated BBB opening might efficiently regulate amyloid beta pathology within a certain range of stimulation.

Cerebral amyloid angiopathy (CAA), characterized by the amyloid deposition around the blood vessel, is found in most patients presenting Alzheimer's disease. The accumulation at the vessel is believed to originate from incomplete clearance of the amyloid from the brain. Previous work has established that accumulation of amyloid in the blood vessels progressively replaces all the different tissues forming the arterial wall[79]. Accumulation of amyloid in the arterial wall affects blood vessel integrity and function, resulting in cerebral infarct or hemorrhage[80]. Post sonication, it was shown that vessels containing amyloid were less susceptible to diameter changes during US/MB-mediated BBB opening protocol, suggesting a more rigid structure. In addition, in a mouse model for AD, small vessels were most likely to display leakage post BBB opening in their littermate controls[26]. Unfortunately, the presence of CAA in patients with AD could be the reason for ineffective anti-amyloid immunotherapy and observed adverse events leading to microhemorrhage in patients[81,82]. In our study, the ARTE10 model also presents some level of CAA, with notable accumulation of amyloid positive staining around the blood vessels (Supp Fig. 3C, Supp fig.4). Targeted analysis did not show any beneficial effect of repeated sonication on the vascular amyloid (Fig 4). However, it is important to note that postmortem brain imaging did not reveal the presence of increased hemorrhage following sonication. This suggests that sonication can

still be a safe and potent strategy to efficiently deliver therapies against amyloid to the brain [23]. As mentioned earlier, few studies have already explored this possibility[4,31–33,35], including during a clinical trial[15]. All studies reported a beneficial effect of therapeutic delivery to the brain and a reduction of the pathology in the different models used (See tables 1 and 2).

Altogether, this study brings additional evidence to the field that repeated sonication to disrupt the BBB is a safe procedure, which could bring positive therapeutic effects in the context of neurodegenerative diseases by both enhancing drug delivery and stimulating mild, transient inflammatory responses. More in-depth analyses are required to understand the molecular and cellular mechanisms at play. However, it is worth considering the therapeutic potential of ultrasound mediated BBB opening in the future, and to explore the synergic effects of their combination to disease modifying therapeutics, which could lead to improved outcomes for patients.

References

1. Yadollahikhales, G. & Rojas, J. C. Anti-Amyloid Immunotherapies for Alzheimer's Disease: A 2023 Clinical Update. *Neurotherapeutics* **20,** 914 (2023).
2. Zhao, P., Zhang, N. & An, Z. Engineering antibody and protein therapeutics to cross the blood–brain barrier. *Antib Ther* **5,** 311 (2022).
3. Trontinemab Data Strengthen Hope for Brain Shuttles | ALZFORUM. at <https://www.alzforum.org/news/conference-coverage/trontinemab-data-strengthen-hope-brain-shuttles>
4. Jordão, J. F., Ayala-Grosso, C. A., Markham, K., Huang, Y., Chopra, R., McLaurin, J. A., Hynynen, K. & Aubert, I. Antibodies Targeted to the Brain with Image-Guided Focused Ultrasound Reduces Amyloid-β Plaque Load in the TgCRND8 Mouse Model of Alzheimer's Disease. *PLoS One* **5,** e10549 (2010).
5. Burgess, A., Huang, Y., Querbes, W., Sah, D. W. & Hynynen, K. Focused ultrasound for targeted delivery of siRNA and efficient knockdown of Htt expression. *Journal of Controlled Release* **163,** 125–129 (2012).
6. Park, J., Aryal, M., Vykhodtseva, N., Zhang, Y. Z. & McDannold, N. Evaluation of permeability, doxorubicin delivery, and drug retention in a rat brain tumor model after ultrasound-induced blood-tumor barrier disruption. *Journal of Controlled Release* **250,** 77–85 (2017).
7. Nisbet, R. M., Van Der Jeugd, A., Leinenga, G., Evans, H. T., Janowicz, P. W. & Götz, J. Combined effects of scanning ultrasound and a tau-specific single chain antibody in a tau transgenic mouse model. *Brain* **140,** 1220–1230 (2017).
8. Karakatsani, M. E., Kugelman, T., Ji, R., Murillo, M., Wang, S., Niimi, Y., Small, S. A., Duff, K. E. & Konofagou, E. E. Unilateral Focused Ultrasound-Induced Blood-Brain Barrier Opening Reduces Phosphorylated Tau from The rTg4510 Mouse Model. *Theranostics* (2019). doi:10.7150/thno.28717
9. Janowicz, P. W., Leinenga, G., Götz, J. & Nisbet, R. M. Ultrasound-mediated blood-brain barrier opening enhances delivery of therapeutically relevant formats of a tau-specific antibody. *Sci Rep* (2019). doi:10.1038/s41598-019-45577-2
10. Meng, Y., Pople, C. B., Huang, Y., Jones, R. M., Ottoy, J., Goubran, M., Oliveira, L. M., Davidson, B., Lawrence, L. S. P., Lau, A. Z., Bethune, A., Maralani, P., Abrahao, A., Hamani, C., Hynynen, K., Kalia, S. K., Lipsman, N. & Kalia, L. V. Putaminal Recombinant Glucocerebrosidase Delivery with Magnetic Resonance–Guided Focused Ultrasound in Parkinson's Disease: A Phase I Study. *Movement Disorders* **37,** 2134–2139 (2022).
11. Trinh, D., Nash, J., Goertz, D., Hynynen, K., Bulner, S., Iqbal, U. & Keenan, J. Microbubble drug conjugate and focused ultrasound blood brain barrier delivery of AAV-2 SIRT-3. *Drug Deliv* **29,** 1176–1183 (2022).
12. Blesa, J., Pineda-Pardo, J. A., Inoue, K. I., Gasca-Salas, C., Balzano, T., López-González Del Rey, N., Reinares-Sebastián, A., Esteban-García, N., Rodríguez-Rojas, R., Márquez, R., Ciorraga, M., del Álamo, M., García-Cañamaque, L., de Aguiar, S. R., Rachmilevitch, I., Trigo-Damas, I., Takada, M. & Obeso, J. A. BBB opening with focused ultrasound in nonhuman primates and Parkinson's disease patients: Targeted AAV vector delivery and PET imaging. *Sci Adv* **9,** (2023).

13. Shen, Y., Zhang, J., Xu, Y., Sun, S., Chen, K., Chen, S., Yang, X. & Chen, X. Ultrasound–enhanced brain delivery of edaravone provides additive amelioration on disease progression in an ALS mouse model. *Brain Stimul* **16,** 628–641 (2023).
14. Arrieta, V. A., Gould, A., Kim, K. S., Habashy, K. J., Dmello, C., Vázquez-Cervantes, G. I., Palacín-Aliana, I., McManus, G., Amidei, C., Gomez, C., Dhiantravan, S., Chen, L., Zhang, D. Y., Saganty, R., Cholak, M. E., Pandey, S., McCord, M., McCortney, K., Castro, B., Ward, R., Muzzio, M., Bouchoux, G., Desseaux, C., Canney, M., Carpentier, A., Zhang, B., Miska, J. M., Lesniak, M. S., Horbinski, C. M., Lukas, R. V., Stupp, R., Lee-Chang, C. & Sonabend, A. M. Ultrasound-mediated delivery of doxorubicin to the brain results in immune modulation and improved responses to PD-1 blockade in gliomas. *Nature Communications 2024 15:1* **15,** 1–19 (2024).
15. Rezai, A. R., D'Haese, P.-F., Finomore, V., Carpenter, J., Ranjan, M., Wilhelmsen, K., Mehta, R. I., Wang, P., Najib, U., Vieira Ligo Teixeira, C., Arsiwala, T., Tarabishy, A., Tirumalai, P., Claassen, D. O., Hodder, S. & Haut, M. W. Ultrasound Blood–Brain Barrier Opening and Aducanumab in Alzheimer's Disease. *New England Journal of Medicine* **390,** 55–62 (2024).
16. Chen, H., Yang, G. Z. X., Getachew, H., Acosta, C., Sierra Sánchez, C. & Konofagou, E. E. Focused ultrasound-enhanced intranasal brain delivery of brain-derived neurotrophic factor. *Scientific Reports 2016 6:1* **6,** 1–8 (2016).
17. Stavarache, M. A., Petersen, N., Jurgens, E. M., Milstein, E. R., Rosenfeld, Z. B., Ballon, D. J. & Kaplitt, M. G. Safe and stable noninvasive focal gene delivery to the mammalian brain following focused ultrasound. *J Neurosurg* **130,** 989–998 (2019).
18. Hynynen, K., McDannold, N., Vykhodtseva, N. & Jolesz, F. A. Noninvasive MR Imaging–guided Focal Opening of the Blood-Brain Barrier in Rabbits1. *https://doi.org/10.1148/radiol.2202001804* **220,** 640–646 (2001).
19. Beccaria, K., Canney, M., Goldwirt, L., Fernandez, C., Adam, C., Piquet, J., Autret, G., Clément, O., Lafon, C., Chapelon, J. Y. & Carpentier, A. Opening of the blood-brain barrier with an unfocused ultrasound device in rabbits. *J Neurosurg* **119,** 887–898 (2013).
20. Horodyckid, C., Canney, M., Vignot, A., Boisgard, R., Drier, A., Huberfeld, G., François, C., Prigent, A., Santin, M. D., Adam, C., Willer, J. C., Lafon, C., Chapelon, J. Y. & Carpentier, A. Safe long-term repeated disruption of the blood-brain barrier using an implantable ultrasound device: a multiparametric study in a primate model. *J Neurosurg* **126,** 1351–1361 (2017).
21. Sabbagh, A., Beccaria, K., Ling, X., Marisetty, A., Ott, M., Caruso, H., Barton, E., Kong, L. Y., Fang, D., Latha, K., Zhang, D. Y., Wei, J., DeGroot, J., Curran, M. A., Rao, G., Hu, J., Desseaux, C., Bouchoux, G., Canney, M., Carpentier, A. & Heimberger, A. B. Opening of the blood–brain barrier using low-intensity pulsed ultrasound enhances responses to immunotherapy in preclinical glioma models. *Clinical Cancer Research* **27,** 4325–4337 (2021).
22. Shen, Y., Hua, L., Yeh, C. K., Shen, L., Ying, M., Zhang, Z., Liu, G., Li, S., Chen, S., Chen, X. & Yang, X. Ultrasound with microbubbles improves memory, ameliorates pathology and modulates hippocampal proteomic changes in a triple transgenic mouse model of Alzheimer's disease. *Theranostics* **10,** 11794–11819 (2020).
23. Noel, R. L., Gorman, S. L., Batts, A. J. & Konofagou, E. E. Getting ahead of Alzheimer's disease: early intervention with focused ultrasound. *Front Neurosci* **17,** (2023).

24. Karakatsani, M. E., Ji, R., Murillo, M. F., Kugelman, T., Kwon, N., Lao, Y. H., Liu, K., Pouliopoulos, A. N., Honig, L. S., Duff, K. E. & Konofagou, E. E. Focused ultrasound mitigates pathology and improves spatial memory in Alzheimer's mice and patients. *Theranostics* **13,** 4102–4120 (2023).
25. Jordão, J. F., Thévenot, E., Markham-Coultes, K., Scarcelli, T., Weng, Y. Q., Xhima, K., O'Reilly, M., Huang, Y., McLaurin, J. A., Hynynen, K. & Aubert, I. Amyloid-β plaque reduction, endogenous antibody delivery and glial activation by brain-targeted, transcranial focused ultrasound. *Exp Neurol* **248,** 16–29 (2013).
26. Burgess, A., Nhan, T., Moffatt, C., Klibanov, A. L. & Hynynen, K. Analysis of focused ultrasound-induced blood-brain barrier permeability in a mouse model of Alzheimer's disease using two-photon microscopy. *Journal of Controlled Release* **192,** 243–248 (2014).
27. Burgess, A., Dubey, S., Yeung, S., Hough, O., Eterman, N., Aubert, I. & Hynynen, K. Alzheimer Disease in a Mouse Model: MR Imaging–guided Focused Ultrasound Targeted to the Hippocampus Opens the Blood-Brain Barrier and Improves Pathologic Abnormalities and Behavior. *https://doi.org/10.1148/radiol.14140245* **273,** 736–745 (2014).
28. Poon, C., McMahon, D. & Hynynen, K. Noninvasive and targeted delivery of therapeutics to the brain using focused ultrasound. *Neuropharmacology* **120,** 20–37 (2017).
29. Bobola, M. S., Chen, L., Ezeokeke, C. K., Olmstead, T. A., Nguyen, C., Sahota, A., Williams, R. G. & Mourad, P. D. Transcranial focused ultrasound, pulsed at 40 Hz, activates microglia acutely and reduces Aβ load chronically, as demonstrated in vivo. *Brain Stimul* **13,** 1014–1023 (2020).
30. Lee, Y., Choi, Y., Park, E. J., Kwon, S., Kim, H., Lee, J. Y. & Lee, D. S. Improvement of glymphatic-lymphatic drainage of beta-amyloid by focused ultrasound in Alzheimer's disease model. *Sci Rep* **10,** (2020).
31. Alecou, T., Giannakou, M. & Damianou, C. Amyloid β Plaque Reduction With Antibodies Crossing the Blood-Brain Barrier, Which Was Opened in 3 Sessions of Focused Ultrasound in a Rabbit Model. *Journal of Ultrasound in Medicine* n/a--n/a (2017). doi:10.1002/jum.14256
32. Antoniou, A., Stavrou, M., Evripidou, N., Georgiou, E., Kousiappa, I., Koupparis, A., Papacostas, S. S., Kleopa, K. A. & Damianou, C. FUS-mediated blood–brain barrier disruption for delivering anti-Aβ antibodies in 5XFAD Alzheimer's disease mice. *J Ultrasound* **27,** 251–262 (2024).
33. Sun, T., Shi, Q., Zhang, Y., Power, C., Hoesch, C., Antonelli, S., Schroeder, M. K., Caldarone, B. J., Taudte, N., Schenk, M., Hettmann, T., Schilling, S., McDannold, N. J. & Lemere, C. A. Focused ultrasound with anti-pGlu3 Aβ enhances efficacy in Alzheimer's disease-like mice via recruitment of peripheral immune cells. *J Control Release* **336,** 443–456 (2021).
34. Deng, Z., Wang, J., Xiao, Y., Li, F., Niu, L., Liu, X., Meng, L. & Zheng, H. Ultrasound-mediated augmented exosome release from astrocytes alleviates amyloid-β-induced neurotoxicity. *Theranostics* **11,** 4351–4362 (2021).
35. Hsu, P. H., Lin, Y. T., Chung, Y. H., Lin, K. J., Yang, L. Y., Yen, T. C. & Liu, H. L. Focused Ultrasound-Induced Blood-Brain Barrier Opening Enhances GSK-3 Inhibitor Delivery for Amyloid-Beta Plaque Reduction. *Scientific Reports 2018 8:1* **8,** 1–9 (2018).

36. Scarcelli, T., Jordão, J. F., O'reilly, M. A., Ellens, N., Hynynen, K. & Aubert, I. Stimulation of Hippocampal Neurogenesis by Transcranial Focused Ultrasound and Microbubbles in Adult Mice. *Brain Stimul* **7,** 304–307 (2014).
37. Mooney, S. J., Shah, K., Yeung, S., Burgess, A., Aubert, I. & Hynynen, K. Focused Ultrasound-Induced Neurogenesis Requires an Increase in Blood-Brain Barrier Permeability. *PLoS One* **11,** e0159892 (2016).
38. Mooney, S. J., Nobrega, J. N., Levitt, A. J. & Hynynen, K. Antidepressant effects of focused ultrasound induced blood-brain-barrier opening. *Behavioural Brain Research* **342,** 57–61 (2018).
39. Pandit, R., Leinenga, G. & Götz, J. Repeated ultrasound treatment of tau transgenic mice clears neuronal tau by autophagy and improves behavioral functions. *Theranostics* **9,** 3754–3767 (2019).
40. Géraudie, A., Riche, M., Lestra, T., Trotier, A., Dupuis, L., Mathon, B., Carpentier, A. & Delatour, B. Effects of Low-Intensity Pulsed Ultrasound-Induced Blood-Brain Barrier Opening in P301S Mice Modeling Alzheimer's Disease Tauopathies. *Int J Mol Sci* **24,** (2023).
41. Meng, Y., MacIntosh, B. J., Shirzadi, Z., Kiss, A., Bethune, A., Heyn, C., Mithani, K., Hamani, C., Black, S. E., Hynynen, K. & Lipsman, N. Resting state functional connectivity changes after MR-guided focused ultrasound mediated blood-brain barrier opening in patients with Alzheimer's disease. *Neuroimage* (2019). doi:10.1016/j.neuroimage.2019.06.060
42. Rezai, A. R., Ranjan, M., D'Haese, P. F., Haut, M. W., Carpenter, J., Najib, U., Mehta, R. I., Chazen, J. L., Zibly, Z., Yates, J. R., Hodder, S. L. & Kaplitt, M. Noninvasive hippocampal blood−brain barrier opening in Alzheimer's disease with focused ultrasound. *Proc Natl Acad Sci U S A* **117,** 9180–9182 (2020).
43. D'Haese, P.-F., Ranjan, M., Song, A., Haut, M. W., Carpenter, J., Dieb, G., Najib, U., Wang, P., Mehta, R. I., Chazen, J. L., Hodder, S., Claassen, D., Kaplitt, M. & Rezai, A. R. β-Amyloid Plaque Reduction in the Hippocampus After Focused Ultrasound-Induced Blood–Brain Barrier Opening in Alzheimer's Disease. *Front Hum Neurosci* **14,** 422 (2020).
44. Epelbaum, S., Burgos, N., Canney, M., Matthews, D., Houot, M., Santin, M. D., Desseaux, C., Bouchoux, G., Stroer, S. & Martin, C. Pilot study of repeated blood-brain barrier disruption in patients with mild Alzheimer's disease with an implantable ultrasound device. *Alzheimers Res Ther* **14,** 1–13 (2022).
45. Tanaka, T., Narazaki, M. & Kishimoto, T. IL-6 in Inflammation, Immunity, and Disease. *Cold Spring Harb Perspect Biol* **6,** 16295–16296 (2014).
46. Angolano, C., Hansen, E., Ajjawi, H., Nowlin, P., Zhang, Y., Thunemann, N., Ferran, C. & Todd, N. Characterization of focused ultrasound blood-brain barrier disruption effect on inflammation as a function of treatment parameters. *Biomedicine & Pharmacotherapy* **182,** 117762 (2025).
47. ARTE10 | ALZFORUM. at <https://www.alzforum.org/research-models/arte10>
48. Kummer, K. K., Zeidler, M., Kalpachidou, T. & Kress, M. Role of IL-6 in the regulation of neuronal development, survival and function. *Cytokine* **144,** 155582 (2021).
49. Choi, B. R., Johnson, K. R., Maric, D. & McGavern, D. B. Monocyte-derived IL-6 programs microglia to rebuild damaged brain vasculature. *Nature Immunology 2023 24:7* **24,** 1110–1123 (2023).
50. Clarke, J. R., Lyra e Silva, N. M., Figueiredo, C. P., Frozza, R. L., Ledo, J. H., Beckman, D., Katashima, C. K., Razolli, D., Carvalho, B. M., Frazão, R., Silveira, M.

A., Ribeiro, F. C., Bomfim, T. R., Neves, F. S., Klein, W. L., Medeiros, R., LaFerla, F. M., Carvalheira, J. B., Saad, M. J., Munoz, D. P., Velloso, L. A., Ferreira, S. T. & De Felice, F. G. Alzheimer-associated Aβ oligomers impact the central nervous system to induce peripheral metabolic deregulation. *EMBO Mol Med* **7,** 190–210 (2015).

51. Lyra e Silva, N. M., Gonçalves, R. A., Pascoal, T. A., Lima-Filho, R. A. S., Resende, E. de P. F., Vieira, E. L. M., Teixeira, A. L., de Souza, L. C., Peny, J. A., Fortuna, J. T. S., Furigo, I. C., Hashiguchi, D., Miya-Coreixas, V. S., Clarke, J. R., Abisambra, J. F., Longo, B. M., Donato, J., Fraser, P. E., Rosa-Neto, P., Caramelli, P., Ferreira, S. T. & De Felice, F. G. Pro-inflammatory interleukin-6 signaling links cognitive impairments and peripheral metabolic alterations in Alzheimer's disease. *Translational Psychiatry 2021 11:1* **11,** 1–15 (2021).
52. Ooi, S. Z. Y., Spencer, R. J., Hodgson, M., Mehta, S., Phillips, N. L., Preest, G., Manivannan, S., Wise, M. P., Galea, J. & Zaben, M. Interleukin-6 as a prognostic biomarker of clinical outcomes after traumatic brain injury: a systematic review. *Neurosurg Rev* **45,** 3035 (2022).
53. Gertz, K., Kronenberg, G., Kälin, R. E., Baldinger, T., Werner, C., Balkaya, M., Eom, G. D., Hellmann-Regen, J., Kröber, J., Miller, K. R., Lindauer, U., Laufs, U., Dirnagl, U., Heppner, F. L. & Endres, M. Essential role of interleukin-6 in post-stroke angiogenesis. *Brain* **135,** 1964–1980 (2012).
54. Lourenco, M. V., Clarke, J. R., Frozza, R. L., Bomfim, T. R., Forny-Germano, L., Batista, A. F., Sathler, L. B., Brito-Moreira, J., Amaral, O. B., Silva, C. A., Freitas-Correa, L., Espírito-Santo, S., Campello-Costa, P., Houzel, J. C., Klein, W. L., Holscher, C., Carvalheira, J. B., Silva, A. M., Velloso, L. A., Munoz, D. P., Ferreira, S. T. & De Felice, F. G. TNF-α mediates PKR-dependent memory impairment and brain IRS-1 inhibition induced by Alzheimer's β-amyloid oligomers in mice and monkeys. *Cell Metab* **18,** 831–843 (2013).
55. Gonzalez Caldito, N. Role of tumor necrosis factor-alpha in the central nervous system: a focus on autoimmune disorders. *Front Immunol* **14,** (2023).
56. Shaftel, S. S., Griffin, W. S. T. & Kerry, K. M. The role of interleukin-1 in neuroinflammation and Alzheimer disease: An evolving perspective. *J Neuroinflammation* **5,** 1–12 (2008).
57. Hewett, S. J., Jackman, N. A. & Claycomb, R. J. Interleukin-1β in Central Nervous System Injury and Repair. *Eur J Neurodegener Dis* **1,** 195 (2012).
58. Tsai, S. J. Effects of interleukin-1beta polymorphisms on brain function and behavior in healthy and psychiatric disease conditions. *Cytokine Growth Factor Rev* **37,** 89–97 (2017).
59. Fetsko, A. R., Sebo, D. J., Budzynski, L. B., Scharbarth, A. & Taylor, M. R. IL-1β disrupts the initiation of blood-brain barrier development by inhibiting endothelial Wnt/β-catenin signaling. *iScience* **27,** (2024).
60. Garcia, J. M., Stillings, S. A., Leclerc, J. L., Phillips, H., Edwards, N. J., Robicsek, S. A., Hoh, B. L., Blackburn, S. & Doré, S. Role of interleukin-10 in acute brain injuries. *Front Neurol* **8,** 253134 (2017).
61. Shemer, A., Scheyltjens, I., Frumer, G. R., Kim, J. S., Grozovski, J., Ayanaw, S., Dassa, B., Van Hove, H., Chappell-Maor, L., Boura-Halfon, S., Leshkowitz, D., Mueller, W., Maggio, N., Movahedi, K. & Jung, S. Interleukin-10 Prevents Pathological Microglia Hyperactivation following Peripheral Endotoxin Challenge. *Immunity* **53,** 1033-1049.e7 (2020).

62. Balzano, T., Pineda-Pardo, J. A., Esteban-García, N., López-Aguirre, M., Reinares-Sebastián, A., Trigo-Damas, I., Takada, M., Obeso, J. A. & Blesa, J. Temporal dynamics of neurovascular unit changes following blood-brain barrier opening in the putamen of non-human primates. *Journal of Controlled Release* **377,** 116–126 (2025).
63. Guo, Y., Lee, H., Kim, C., Park, C., Yamamichi, A., Chuntova, P., Gallus, M., Bernabeu, M. O., Okada, H., Jo, H. & Arvanitis, C. Ultrasound frequency-controlled microbubble dynamics in brain vessels regulate the enrichment of inflammatory pathways in the blood-brain barrier. *Nature Communications 2024 15:1* **15,** 1–17 (2024).
64. Rigollet, S., Rome, C., Ador, T., Dumont, E., Pichon, C., Delalande, A., Barbier, E. L. & Stupar, V. FUS-mediated BBB opening leads to transient perfusion decrease and inflammation without acute or chronic brain lesion. *Theranostics* **14,** 4147–4160 (2024).
65. Liu, T., Zhang, L., Joo, D. & Sun, S. C. NF-κB signaling in inflammation. *Signal Transduction and Targeted Therapy 2017 2:1* **2,** 1–9 (2017).
66. Xu, G., Dong, F., Su, L., Tan, Z. X., Lei, M., Li, L., Wen, D. & Zhang, F. The role and therapeutic potential of nuclear factor κB (NF-κB) in ischemic stroke. *Biomedicine & Pharmacotherapy* **171,** 116140 (2024).
67. Roberts, T. K., Eugenin, E. A., Lopez, L., Romero, I. A., Weksler, B. B., Couraud, P. O. & Berman, J. W. CCL2 disrupts the adherens junction: implications for neuroinflammation. *Laboratory Investigation 2012 92:8* **92,** 1213–1233 (2012).
68. Schellenberg, A. E., Buist, R., Del Bigio, M. R., Toft-Hansen, H., Khorooshi, R., Owens, T. & Peeling, J. Blood-brain barrier disruption in CCL2 transgenic mice during pertussis toxin-induced brain inflammation. *Fluids Barriers CNS* **9,** 1–9 (2012).
69. Guo, F., Xu, D., Lin, Y., Wang, G., Wang, F., Gao, Q., Wei, Q. & Lei, S. Chemokine CCL2 contributes to BBB disruption via the p38 MAPK signaling pathway following acute intracerebral hemorrhage. *FASEB J* **34,** 1872–1884 (2020).
70. Dimitrijevic, O. B., Stamatovic, S. M., Keep, R. F. & Andjelkovic, A. V. Effects of the chemokine CCL2 on blood-brain barrier permeability during ischemia-reperfusion injury. *J Cereb Blood Flow Metab* **26,** 797–810 (2006).
71. Liu, Z., Zhang, H., Lu, K., Chen, L., Zhang, Y., Xu, Z., Zhou, H., Sun, J., Xu, M., Ouyang, Q., Thompson, G. J., Yang, Y., Su, N., Cai, X., Cao, L., Zhao, Y., Jiang, L., Zheng, Y. & Zhang, X. Low-intensity pulsed ultrasound modulates disease progression in the SOD1G93A mouse model of amyotrophic lateral sclerosis. *Cell Rep* **43,** 114660 (2024).
72. Kovacsa, Z. I., Kima, S., Jikariaa, N., Qureshia, F., Miloa, B., Lewisa, B. K., Breslera, M., Burksa, S. R. & Franka, J. A. Disrupting the blood-brain barrier by focused ultrasound induces sterile inflammation. *Proc Natl Acad Sci U S A* **114,** E75–E84 (2017).
73. McMahon, D. & Hynynen, K. Acute Inflammatory Response Following Increased Blood-Brain Barrier Permeability Induced by Focused Ultrasound is Dependent on Microbubble Dose. *Theranostics* **7,** 3989 (2017).
74. Chang, J. W., Wu, M. T., Song, W. S. & Yang, F. Y. Ultrasound Stimulation Suppresses LPS-Induced Proinflammatory Responses by Regulating NF-κB and CREB Activation in Microglial Cells. *Cerebral Cortex* **30,** 4597–4606 (2020).
75. Rauti, R., Cellot, G., D'Andrea, P., Colliva, A., Scaini, D., Tongiorgi, E. & Ballerini, L. BDNF impact on synaptic dynamics: extra or intracellular long-term release differently

regulates cultured hippocampal synapses. *Molecular Brain 2020 13:1* **13,** 1–16 (2020).
76. Cirrito, J. R., Yamada, K. A., Finn, M. B., Sloviter, R. S., Bales, K. R., May, P. C., Schoepp, D. D., Paul, S. M., Mennerick, S. & Holtzman, D. M. Synaptic Activity Regulates Interstitial Fluid Amyloid-β Levels In Vivo. *Neuron* **48,** 913–922 (2005).
77. Li, X., Uemura, K., Hashimoto, T., Nasser-Ghodsi, N., Arimon, M., Lill, C. M., Palazzolo, I., Krainc, D., Hyman, B. T. & Berezovska, O. Neuronal activity and secreted amyloid β lead to altered amyloid β precursor protein and presenilin 1 interactions. *Neurobiol Dis* **50,** 127–134 (2013).
78. Kazim, S. F., Seo, J. H., Bianchi, R., Larson, C. S., Sharma, A., Wong, R. K. S., Gorbachev, K. Y. & Pereira, A. C. Neuronal Network Excitability in Alzheimer's Disease: The Puzzle of Similar versus Divergent Roles of Amyloid β and Tau. *eNeuro* **8,** (2021).
79. Keable, A., Fenna, K., Yuen, H. M., Johnston, D. A., Smyth, N. R., Smith, C., Salman, R. A. S., Samarasekera, N., Nicoll, J. A. R., Attems, J., Kalaria, R. N., Weller, R. O. & Carare, R. O. Deposition of amyloid β in the walls of human leptomeningeal arteries in relation to perivascular drainage pathways in cerebral amyloid angiopathy. *Biochim Biophys Acta* **1862,** 1037–1046 (2016).
80. Smith, E. E. & Greenberg, S. M. β-Amyloid, blood vessels, and brain function. *Stroke* **40,** 2601–2606 (2009).
81. Sveikata, L., Charidimou, A. & Viswanathan, A. Vessels Sing Their ARIAs: The Role of Vascular Amyloid in the Age of Aducanumab. *Stroke* **53,** 298–302 (2022).
82. Taylor, X., Clark, I. M., Fitzgerald, G. J., Oluoch, H., Hole, J. T., DeMattos, R. B., Wang, Y. & Pan, F. Amyloid-β (Aβ) immunotherapy induced microhemorrhages are associated with activated perivascular macrophages and peripheral monocyte recruitment in Alzheimer's disease mice. *Mol Neurodegener* **18,** (2023).

Experimental Procedures

Pharmacological compounds used:

Ketamine (Zetamine: VetOne, catalogue No. AH202C6)/xylazine (Rompun: Bayer, catalogue No. AH200W5) anesthesia was formulated in sterile phosphate buffered saline (PBS: Corning Cellgro, catalogue No. 21-031-CV) for IP injection at 10 µL/gram (90 mg/kg ketamine / 10 mg/kg xylazine) as follows: Ketamine/xylazine mixture, Ketamine (100 mg/ml, 0.9 mL), Xylazine (100 mg/ml, 0.1 mL), Saline (9.0 mL). Revertidine (atipamezole: Modern Veterinary Therapeutics, catalogue No. 023575) was formulated in PBS for IP injection at 2 µL/gram as follows: Atipamezole mixture, Atipamezole (5 mg/mL, 0.5 mL), Saline (4.5 mL). Lumason microbubbles (Bracco Diagnostics, catalogue No. 20A108A) were prepared for RO injection, initially at 200 µL/mouse and then decreased to 100 uL/mouse according to the manufacturer's instructions. All compounds were stored at room temperature when not in use. See the study protocol (Appendix C) for additional details of compound preparation, dosing, and storage.

Mouse models

Male C57BL/6J mice (N = 20 + 3 extra) that were approximately 17 weeks of age were obtained from The Jackson Laboratory (Bar Harbor, ME). 1 year old femelles of ARTE10 mouse model was used as a model for amyloid pathology. This model has two mutations in APP and PSEN1, similar to the APP/PS1dE9 model. ARTE10 mice are characterized by a robust amyloid deposition from 3 months old, associated with an early synaptic loss at 3 months old, gliosis at 6 months old and cognitive impairment at 12 months old. ARTE10-Model 16347 were obtained from Taconic (N = 36 + 2 extras). The mice weighed approximately 27 to 31 grams (mean 30 g) on study day 0. Main study animals were identified by color-coded dots at the base of the tail delineating group and animal number. After randomization, all cages were labeled with protocol number, group number, and animal numbers with the appropriate color-coding.

Environment and Husbandry

Main study mice were housed 2 to 5 per cage in polycarbonate cages with wood chip bedding and suspended food and water bottles. The mice were housed either in shoebox cages (static airflow, approximately 0.045 m2 floor space) with filter tops or in individually ventilated pie cages (passive airflow, approximately 0.045-0.048 m2 floor space). Animal care including room, cage, and equipment sanitation conformed to the guidelines cited in the Guide for the Care and Use of Laboratory Animals (Guide, 2011) and the applicable Inotiv Boulder SOPs. Main study mice were acclimated for 7 days prior to being placed in the study. An attending veterinarian was on site or on call during the live phase of the study. No concurrent medications were given. During the acclimation and study periods, the animals were housed in a laboratory environment with temperatures ranging 19°C to 25°C and relative humidity of 30% to 70%. Automatic timers provided 12 hours of light and 12 hours of dark. The animals were allowed access ad libitum to Envigo Teklad 8640 diet and fresh municipal tap water.

Sonication

The following ultraound parameters were used: 120□seconds using a 1-MHz 25,000-cycle burst at a 1□Hz pulse repetition frequency and an acoustic pressure of 0.3□MPa predefined in the ultrasound device (Carthera, France). To prepare for sonication, hair on the head of all

animals was removed using Nair™. At the time of sonication, mice were administered 5 µL/gram anesthesia i.p. (ketamine -xylanine). Lumason microbubbles were injected in the retro-orbital sinus (r.o.) at a dose of 150 µL/mouse and mice underwent a single sonication event. Mice were given 10 mg/kg atipamezole (Rivertidine; Modern Veterinary Therapeutics, Cat #023575) i.p. within 20 min of ketamine administration to reverse the anesthesia. After 15 min, blood was collected for PK.

Experimental Design for WT animals

On study day 0, the animals were weighed and randomized into groups as indicated in the following table. Additionally, animals were weighed on study days 0, 1, 7, and 14. The animals' heads were shaved and all hair on the head was removed using Nair™. A pre-sonication blood sample was collected on study day 0. On study day 1, the animals received a single sonication event in combination with RO-injected microbubbles (200 µL/mouse) while under ketamine/xylazine anesthesia. After sonication, the animals were woken up with atipamezole. All animals were bled by retro-orbital blood draw for plasma (EDTA) on study day 0 (baseline; 120 µL of plasma/mouse). Plasma samples were stored frozen at −80°C for analysis of S100. The animals were euthanized for necropsy and terminal sample collection 1 day, 3 days, 7 days, or 14 days post-sonication/microbubble injection as described in the next table. Group and Treatment Information:

Group	N	Treatment	Dose Level (µL/mouse)	Route	Regimen	Dosing days	Necropsy Time (days post-sonication)
1	5	Microbubbles (Sonovue/Lumason)	200	RO	1x	Day 1	1 day
2	5	Microbubbles (Sonovue/Lumason)	200	RO	1x	Day 1	3 days
3	5	Microbubbles (Sonovue/Lumason)	200	RO	1x	Day 1	7 days
4	5	Microbubbles (Sonovue/Lumason)	200	RO	1x	Day 1	14 days

Experimental Design for ARTE10 animals

On study day 0, the animals were weighed and randomized into groups as indicated in table below. Additionally, animals were weighed and clinical observations were recorded on D0, D7, D14, D21, D28, and D49. The animals' heads were shaved and all hair on the head was removed using Nair™. A pre-sonication blood sample was collected on study day 0. On study day 1, the animals received a single sonication event in combination with RO-injected microbubbles (200 µL/mouse, later changed to 100 µL/mouse according to the manufacturer's instructions) while under ketamine/xylazine anesthesia. After sonication, the

Group	**N**	**Disease**	**Sex**	**Treatment**	**Necropsy**

animals were woken up with atipamezole. Group and Treatment Information:

1	6	AD	M	None; ctrl	1 wk after last sonication
2	6	AD	M	None; ctrl	1 month after last sonication
3	6	AD	M	Sparse sonication (0.5x/week*8 =4 total sonications)	1 wk after last sonication
4	6	AD	M	Dense sonication (2x/week*4 =8 total sonications)	1 wk after last sonication
5	6	AD	M	Sparse sonication (0.5x/week*8 =4 total sonications)	1 month after last sonication
6	6	AD	M	Very sparse sonication (0.5x/week*8 =2 total sonications)	1 wk after last sonication

Blood Collection and Processing

Whole blood (150 µL in EDTA yielding 75 µL plasma on D0 and D1; 200 µL in EDTA yielding 100 µL plasma all other bleed days) for PK was collected via r.o. puncture under isoflurane anesthesia 15 min following sonication. All animals in Groups 2, 4, and 6 had blood collected twice on D0 (before and after sonication), then once on D7, D14, and D21; all animals in Group 1, 3, and 5 had blood collected twice on D1 (before and after sonication), then once on D8, D15, and D22. Blood samples were processed to produce plasma and stored at -80 °C until assayed at Inotiv Boulder (Inotiv Boulder (formerly Bolder BioPATH, Inc.), 5541 Central Ave., Suite 160, Boulder, CO 80301). Final blood (≥ 800 µL in EDTA yielding ≥ 400 µL plasma) was collected via direct cardiac puncture at necropsy and processed to produce plasma. Plasma samples were stored at -80 °C until assayed at Inotiv Boulder.

Postmortem tissue collection

The animals were necropsied on day 2 (group 1), day 4 (group 2), day 8 (group 3), or day 15 (group 4) following sonication on day 1. At necropsy, the animals were overdosed with ketamine (100 mg/kg)/xylazine (10 mg/kg) and bled to exsanguination followed by cervical dislocation. Brains were halved along the longitudinal fissure. Right brain hemispheres were fixed in 4% PFA, then transferred to 40% sucrose/saline the next day and stored at 4°C for histology. Left brain hemispheres were collected into RNase/DNase free clean tubes and stored at −80°C for gene expression analysis. Cerebrospinal fluid (CSF) samples were collected and whole blood was collected and processed to plasma (EDTA, 300 µL/mouse). Plasma and CSF samples (5-10 µL/mouse) were stored at −80°C for analysis. Whole blood samples (300 µL/mouse) were also collected and stored at room temperature for shipment to Antech.

Clinical Pathology Methods

Whole blood for complete blood counts (CBCs) was shipped to Antech Diagnostics (details) for analysis. The following parameters were analyzed.

CBC Analysis:

Total leukocyte count (WBC)	Absolute Monocyte count
Absolute Erythrocyte count (RBC)	Absolute Eosinophil Count
Hemoglobin concentration (HGB)	Absolute Basophil Count
Hematocrit value (HCT)	Neutrophil Percentage
Mean corpuscular volume (MCV)	Lymphocyte Percentage
Mean corpuscular hemoglobin (MCH)	Monocyte Percentage
Mean corpuscular hemoglobin concentration (MCHC)	Eosinophil Percentage
	Basophil Percentage
Absolute Neutrophil count	Platelet count (PLT)
Absolute Lymphocyte count	

ELISA Methods

For WT animals:

Plasma samples were analyzed for S100 using a Mouse Protein S100B/S100 Beta ELISA Kit (CUSABio, catalogue No. CSB-EL020643MO, lot No. J16147391). ELISA data can be found in Table 3. The assay was performed in accordance with the kit instructions. All reagents and samples were brought to room temperature without additional heating and mixed thoroughly by gently swirling before pipetting (to avoid foaming). All reagents, working standards, and samples were prepared as directed in the kit instructions.

For ARTE10 Cohort:

S100 calcium-binding protein beta (S100-β) concentrations were determined in duplicate using a commercially available mouse S100-β enzyme-linked immunosorbent assay (ELISA) kit (LSBio #LS-F5980). S100-β was assayed according to the manufacturer's specifications. Samples and standards were added to separate wells of a 96-well plate pre-coated with an anti-S100-β antibody and incubated at 37 °C for 60 min followed by aspiration. Subsequently, Detection Reagent A was added to all wells and incubated at 37 °C for 60 min with agitation followed by a wash cycle. Detection Reagent B was added to all wells and incubated at 37 °C for 30 min followed by a wash cycle. Then, TMB Substrate was added to all wells and incubated at 37 °C for 10 – 20 min, protected from light. Finally, Stop Solution was added to each well. Absorbance was read at 450 nm.

Real-Time Quantitative Polymerase Chain Reaction (RT-qPCR) Methods

For WT animals:

RT-qPCR analysis was performed on left brain hemispheres from all animals. Tissue samples (approx. 30 mg each) were weighed out and homogenized in 600 µL of RLT buffer on a FastPrep-24 5G. Supernatants were spun and transferred to a new tube for RNA isolation. RNA was isolated using a Qiagen RNeasy Mini kit (No. 74106) and the manufacturer-recommended protocol, quantified on a NanoDrop spectrophotometer, and 500 ng of RNA (when available) was reverse transcribed into cDNA using the ThermoFisher High Capacity cDNA kit (ThermoFisher, No. 4368814). cDNA samples were then analyzed using Taqman primers against *cyc1*, *cxcl1*, *ccl2*, *Il-1β*, *Il-6*, *tnf-a*, *Icam*, *Il-10*, *tgf-β*, *Il-13*, *bdnf*, *nf-κb*, *p-Selectin*, *e-Selectin*, GM-CSF, and G-CSF. All primers were selected from validated

primer sets from ThermoFisher Scientific. Recorded CT values were recorded and means for *cxcl1*, *ccl2*, *Il-1β*, *Il-6*, *tnf-α*, *iCAM*, *Il-10*, *tfg-β*, *Il-10*, *bdnf*, *nf-κb*, *e-Selectin*, were calculated.

For ARTE10 cohort:
Multiplex qPCR master mix was prepared using TaqMan Multiplex Master Mix (ThermoFisher, Cat #4484263) according to manufacturer's specifications for 96-well plates. Samples were run in triplicate for the following genes: *interleukin 1 beta* (*Il-1β*), *interleukin 6* (*Il-6*), *tumor necrosis factor alpha* (*tnf-α*), *brain-derived neurotrophic factor* (*bdnf*), *CC motif chemokine ligand 2* (*ccl2*), *intercellular adhesion molecule* (*Icam*),

Histological Processing
Mouse hemibrains (n = 31) were trimmed to remove olfactory bulbs, divided into 6-piece coronal sections, and paraffin embedded frontal side down. Pieces 1, 3, and 5 were embedded in a single block and pieces 2, 4, and 6 were embedded in a single block to equal 2 blocks per brain sample for a total of 62 blocks. Brain sections were mounted on glass slides and stained with hematoxylin and eosin (H&E) using standard methods.
For immunohistochemical (IHC) staining of mouse hemibrains, staining was conducted on the Leica Bond RXm platform using standard chromogenic methods. For antibodies requiring heat induced epitope retrieval (HIER), slides were heated in a pH9 ethylenediaminetetraacetic acid (EDTA)-based buffer at 94 °C for 25 min followed by primary antibody incubation for 30 or 60 min. Antibody binding was detected using an anti-rabbit horseradish peroxidase (HRP)-conjugated secondary polymer, followed by chromogenic visualization with diaminobenzidine (DAB). A hematoxylin counterstain was used to visualize nuclei.

Immunohistochemistry Antibody Information.

Target	Host	Clone	Vendor	Cat #	Stock Conc. (mg/mL)
Iba1	Rabbit	EPR16588	AbCam	ab178846PUR	1.272
GFAP	Rabbit	EPR1034Y	AbCam	ab68428	0.046
Aβ	Rabbit	D12B2	Cell Signaling	9888	0.194
CD3	Rabbit	SP7	AbCam	ab16669	???

Immunohistochemical Staining Parameters.

Antibody	Antigen Retrieval	Dilution	Working conc (ug/ml)	Chromogen
Iba1	pH9	1:40,000	0.0318	DAB
GFAP	pH9	1:200	0.2300	DAB
Aβ	pH9	1:200	0.9700	DAB

CD3	pH9	1:100	–	DAB

Image Analysis

IHC-stained glass slides (n = 62) labelled for Aβ were scanned using an Aperio AT2 whole slide scanner with a maximum objective of 20x (200x total magnification). Image analysis was conducted on Aβ IHC-stained digital slide images using Visiopharm® software. Image analysis, including annotations and algorithm development, was supervised by Laura Hoon-Hanks, D.V.M., Ph.D., D.A.C.V.P., a board-certified veterinary pathologist.

Six coronal sections of brain per animal (across 2 slides) were annotated manually as individual regions of interest (ROIs): rostral 1 and 2, middle 1 and 2, and caudal 1 and 2. The meninges as well as areas of tissue/staining artifact were excluded from analysis. For quantification of Aβ immunolabeling area, a threshold of analysis was utilized to classify IHC positivity within tissue. Color deconvolution based on diaminobenzidine (DAB) staining was used to develop and implement the threshold. IHC-positive area and total area within each ROI were used to calculate percent positive area for Aβ immunolabeling. The calculations for percent positive area (%) are provided below:

□□□□□□□ □□□□□□□□□ □□□a (%)=□□□□□□□□□ □□□□ (μ□2)/□□□□□ □□□□ (μ□2)□ 100

Imaging and Analytical Methods

Whole slide images previously scanned were provided by the designer. Whole slide images were then imported into Visiopharm software (version 2022.12) for further analysis. First, a deep learning algorithm trained to detect tissue was run on each slide to define the region of interest (ROI). Deep learning algorithms (DLA) use convolutional neural networks (CNNs) that can be trained to identify specific objects within the tissue based on morphological patterns, RGB signatures, texture, size, and spatial relationships. This algorithm was developed using the U-Net model. This model utilizes large tile overlap, thereby allowing training data to be limited to a single image rather than requiring large batch analyses. During training, U-Net also incorporates random rotation, flipping, brightness, and contrast factors for data augmentation.

AB IHC

A second DLA trained to detect vascular endothelium trained on slides stained with β-amyloid IHC was used to define vessels. These vessels were then outlined into a separate ROI.

b-amyloid immunolabeling was detected using a final DLA. AB signal was assessed as total, plaque and non-plaque. Plaques were defined as areas of dense β-amyloid immunolabeling 200 m2 in area resulting in distortion of the surrounding cellular architecture. Non-plaque immunolabeling was present as fibers in aggregate or dispersed in the neuropil, as intracellular/neuronal immunolabeling, and in blood vessel walls. Total β-amyloid burden was defined by the sum of the areas of plaques and non-plaques. For the frontal cortex segmentation, data were reported as percent area of total AB, percent area of plaques, number of plaques, and average plaque size. These data were reported from total brain area, including all 6 sections of the brain including vasculature, as well as frontal cortex as defined by the Allen Brain Atlas. Three of the 6 sections had frontal cortex present.

All calculations were performed in Excel. Total brain area was defined as the sum of the brain area (ROI1, green) and the vascular area (ROI2, teal). Total brain β-amyloid plaque and fiber area was defined as the sum of the area of the blue label (fiber) and red label (plaque) in both ROIs. Vascular area and β-amyloid positivity were a subset of this data. For the frontal cortex segmentation, total brain area was defined as the sum of non-frontal cortex brain area (ROI1, green), the vascular area (ROI2, teal), and the frontal cortex (ROI3, red).

CD3, GFAP, and IBA1 IHC

CD3, GFAP, and IBA1 immunolabeling was detected using thresholding techniques. All three thresholds were developed individually based on Visiopharm's proprietary HDAB filter, which isolates the specific intensity and colorimetric signature associated with positive DAB-based immunolabeling.

All calculations were performed in Excel. For these labels, the vasculature was not individually isolated. Total brain area was defined as the sum of the non-frontal cortex brain area (ROI1, green) and the frontal cortex (ROI1, red). Further, only 4 sections were analyzed rather than all 6; sections with cerebellum and far hindbrain were excluded. CD3 quantification is reported as positive cell density/mm2; GFAP and IBA1 quantification is reported as positive percent area.

Statistical Analyses

Statistical analyses were performed on the data generated from this study using GraphPad Prism 10.03 for Windows (GraphPad Software, Inc.). Details of each analysis can be found in the figure legend presenting the data. Statistical significance was set at $p < 0.05$.

Figure Legends:

Figure 1: Physiological consequence of a single session of ultrasound mediated BBB-opening: A) Schematic summarizing the key steps of the protocole. Briefly, wildtype mice were first weighed and a blood sample collected before undergoing a single sonication procedure. 4 groups of mice were followed with terminal points at 2-, 4-, 8- and 15-days post sonication. During this time, mouse weights were monitored. At sacrifice, a blood sample was collected, and brains were harvested for ex vivo analyses. **B)** Graphic plots representing the complete blood count, each dot representing one animal. Red blood and White blood cells number were counted in the final collected blood sample (number of cells expressed in nx10^3 for white blood cells and nx10^6 for red blood cells, left Y axis). Hemoglobin levels and Mean corpuscular hemoglobin concentration (MCHC) was measured (in ng/dl, right Y axis). 2-way ANOVA with post hoc Tukey's multiple comparison test, difference between groups $F (3, 12) = 2.923$, $P=0.0773$ **C)** Graphic plots representing the complete blood count, each dot representing one animal. Number of neutrophils, lymphocytes, monocytes, eosinophils and basophils were counted for each group (in cells per microliter). 2-way ANOVA with post hoc Tukey's multiple comparison test, difference between groups $F (12, 48) = 0.8972$, $P=0.5560$ **D)** Heatmap representing the RT-Q-PCR quantification performed on extracted brains for different markers and normalized by the control group. The legend on the left indicates the level of increase or decrease compared to the Mean of the control group. Colors are based on the Median. P value in each cell

indicates the significance compared to the control group, mixed effect analysis with post hoc dunnett's multiple comparison test, difference between groups F (4, 18) = 25.68, p<0.0001.

Table 1: Row Statistics for the heatmap (Fig1D): Table summarizing for each group the mean, SD and N for the different markers analyzed. Triplicates were averaged per mouse.

Figure S1: Health check and BBB opening markers: A) line graph representing the evolution of the mouse weight for each group. Each line represents an individual mouse. Group 1 (blue) and group 2 (orange) only have 2 measurements, with a respective sacrifice at day 2 and day 4 post sonication. Mixed effect analysis with post hoc Sidak's multiple comparisons test, difference between timepoints F (0.1883, 1.569) = 5.678, P=0.06277 **B)** Arrow plot representing the level of S100b just after BBB opening and at sacrifice. Mixed effect analysis with post hoc Sidak's multiple comparisons test, difference between timepoints F (1, 12) = 10.91, P=0.0063.

Figure 2: Physiological data on the ARTE10 cohort following repeated sonication protocols: A) Schematic summarizing the experimental plan for the different groups (1 to 6), the sonication schedule and sacrificing date following the last sonication session. **B)** Line graph representing the evolution of the median weight for each group (bars represent the range). No significance was observed between groups, mixed effects analysis at 1 week: F (3, 20) = 0.5542, P=0.6513m at 1 month: F (1, 10) = 3.214, p=0.1033. **C and D)** line graph representing level of serum S100b measured by ELISA at the different timepoints. No significant differences were observed between groups, mixed effects analysis, at 1 week **(C)**: difference between groups F (3, 113) = 1.782, P=0.1546, at 1 month **(D)**: difference between groups F (1, 71) = 0.7472, P= 0.3903.

Figure 3: Inflammatory cellular landscape of the brain following repeated sonication procedures: A) Representative image showing the presence of CD3+, GFAP+ and Iba1+ cells around an amyloid deposit, labelled with a b-amyloid antibody. **B)** Representative images showing the presence of T-cells (CD3+) present in the brain parenchyma of the different group. **C)** Box plot showing median and min/max values for the density of T-cells (CD3+) present in the brain parenchyma of the different group. No significant differences between groups were recorded, 2-way ANOVA with post hoc Tukey's multiple comparisons test, difference between groups F (5, 25) = 1.285, P=0.3016. **D)** Representative images showing the occupancy of astrocytes (GFAP+) in the brain parenchyma of the different groups. **E)** Representative images showing the occupancy of microglial (Iba1+) in the brain parenchyma of the different groups. **F)** Box plot showing median and min/max values for the total occupancy for astrocytes (purple bars) and microglia (yellow bars) in the brain parenchyma of the different groups. No significant differences between groups were recorded, 2-way ANOVA with post hoc Tukey's multiple comparisons test, difference between groups F (5, 25) = 1.280, P=0.3038.

Supplemental Figure 2: automated image analysis pipeline and inflammatory marker expression post repeated sonication protocol: A-C) Representative example of the automated pipeline allowing detection of CD3+ cell **(A)**, GFAP **(B)** and Iba1 **(C)**. Positive cells are highlighted in red, allowing the quantification of the number of CD3+ per mm2 and the surface of occupancy for GFAP and Iba1 positive cells. **D)** heatmap representing the preliminary RT-Q-PCR dataset collected at each timepoint and exploring the level of

inflammatory markers post repeated sonication. No statistical analyses were performed due to the lack of independent data available.

Table 2: Row Statistics for the heatmap (Supp Fig3D): Table summarizing for each group the mean, SD and N for the different markers analyzed. As several data were missing, we analyzed Nplicates from different mice, but did not express the data per mouse for each groups.

Figure 4: Decrease of the amyloid load following monthly sonication regimen: A) Representative images of the hippocampal region isolated from immunohistochemistry staining of b-amyloid on coronal sections. **B)** Bar graph representing the total amyloid load (in percentage of positive area) for each group. Each dot represents an independent animal from the group. One-way ANOVA with post hoc Tukey's multiple comparisons test, F(3, 16)=0.04014, p=0.0163. **C)** Heatmap representing the level of amyloid deposition in the brain at different locations from rostral to caudal. Pseudo coloring represents the Median of each group. 2-way ANOVA, difference between groups F (5, 25) = 3.323, P=0.0195. D) Box plot showing median and min/max values for the total amyloid positive area (red boxes), amyloid deposits (green boxes) and vascular amyloid deposition (yellow boxes). 2-way ANOVA with post hoc Tukey's multiple comparisons test, difference between groups F (5, 25) = 4.317, P=0.0057.

Table 3: Row Statistics for the heatmap (Fig4C): Table summarizing for each group the mean, SD and N for the different locations analyzed. Triplicates were averaged per mouse.

Supplemental Figure 3: Pathology of the ARTE10 and supplemental analyses for the effect of a monthly sonication regimen: A) Representative images showing different types of pathological deposition, with the amyloid deposits (left) and the mineralized deposits (right, M). **B)** Representative images showing loss of hippocampal neurons in the cellular layer of the dentate gyrus. Arrows point at the area showing loss of neuronal cell bodies. H=hippocampus, C=cortex, M=molecular layer, G=granular layer, P=polymorphic layer. **C)** Representative images highlighting the presence of amyloid deposition around the brain vasculature. Arrows point at the vascular deposition, observed on serial sections. **D)** Side by side comparison of group 1 (control) and group 6 (very sparse sonication), highlighting the effect of the monthly sonication. Number of amyloid deposits (per mm2), percentage of amyloid positive area and amyloid deposits area was compared between the two groups. For all the comparisons, Group1 and Group6 were compared using nonparametric multiple t-test Mann-Whitney. Graphical representations show median and min/max values, statistical values show calculated q-value. Percentage of b-amyloid deposit area, total, group 1 vs group 6, p=0.1143, q=0.1154; Frontal cortex, group 1 vs group 6, p=0.1143, q=0.1154. Average deposits area, total, group 1 vs group 6, p=0.019, q=0.0385; Frontal cortex, group 1 vs group 6, p=0.1143, q=0.1154.

Supplemental Figure 4: Artificial intelligence quantification of amyloid pathology: Representative images showing the total amyloid load by immunohistochemistry and pseudo color from the automated quantification pipeline, as well as the vascular amyloid deposition by immunohistochemistry and pseudo color from the automated quantification pipeline.

Table 4: List of the previous mouse models used in combination with Ultrasound. Four models have been used to explore the effect of sonication on the amyloid pathology

Table 5: Previous studies using ultrasound in mouse models for Alzheimer's Disease and their output.

Supplemental Figures 5 to 10: Full brain scans of each groups, respectively Group 1 – SuppFig5, Group 2 – Supp Fig 6, Group 3 – Suppl Fig 7, Group 4 – Suppl Fig 8, Group 5 – Suppl Fig 9, Group 6 – Suppl Fig 10

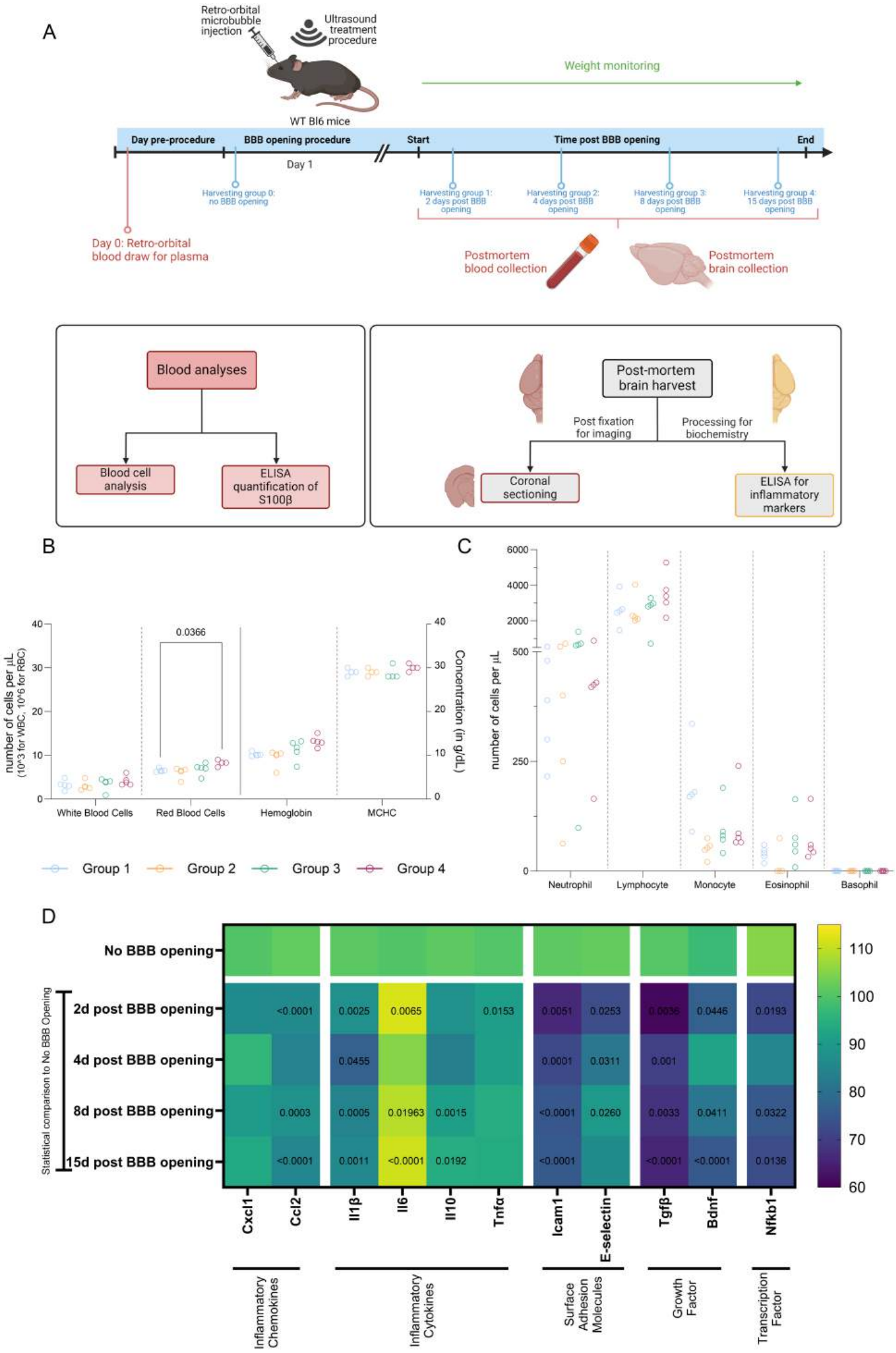
A
Retro-orbital microbubble injection
Ultrasound treatment procedure
WT Bl6 mice
Weight monitoring
Day pre-procedure
BBB opening procedure
Day 1
Start
Time post BBB opening
End
Harvesting group 0: no BBB opening
Harvesting group 1: 2 days post BBB opening
Harvesting group 2: 4 days post BBB opening
Harvesting group 3: 8 days post BBB opening
Harvesting group 4: 15 days post BBB opening
Day 0: Retro-orbital blood draw for plasma
Postmortem blood collection
Postmortem brain collection
Blood analyses
Blood cell analysis
ELISA quantification of S100β
Post-mortem brain harvest
Post fixation for imaging
Processing for biochemistry
Coronal sectioning
ELISA for inflammatory markers
B
number of cells per µL (10^3 for WBC, 10^6 for RBC)
Concentration (in g/dL)
0.0366
White Blood Cells
Red Blood Cells
Hemoglobin
MCHC
Group 1
Group 2
Group 3
Group 4
C
number of cells per µL
Neutrophil
Lymphocyte
Monocyte
Eosinophil
Basophil
D
No BBB opening
2d post BBB opening
4d post BBB opening
8d post BBB opening
15d post BBB opening
Statistical comparison to No BBB Opening
Cxcl1
Ccl2
Il1β
Il6
Il10
Tnfα
Icam1
E-selectin
Tgfβ
Bdnf
Nfkb1
Inflammatory Chemokines
Inflammatory Cytokines
Surface Adhesion Molecules
Growth Factor
Transcription Factor

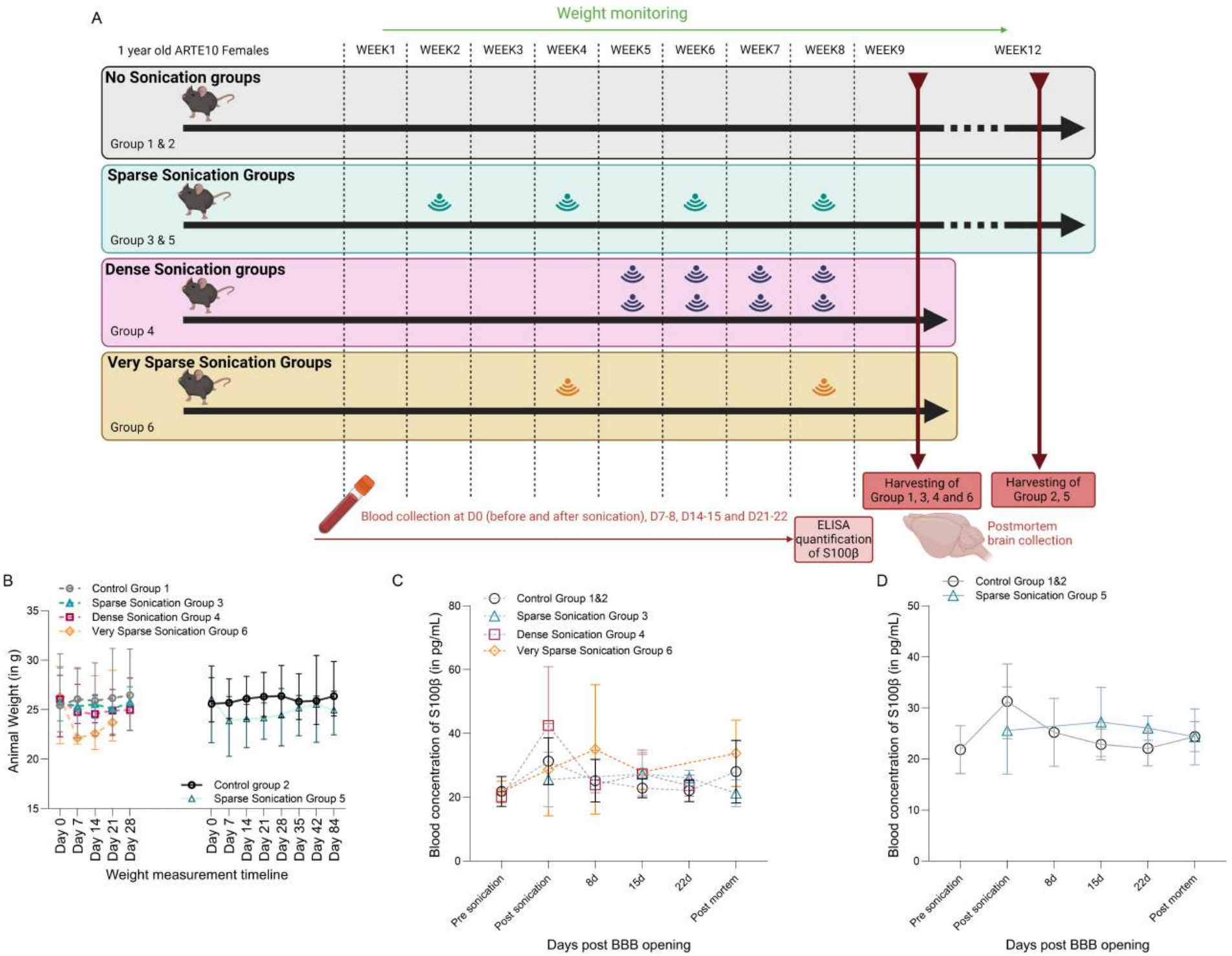
A
Weight monitoring
1 year old ARTE10 Females
WEEK1
WEEK2
WEEK3
WEEK4
WEEK5
WEEK6
WEEK7
WEEK8
WEEK9
WEEK12
No Sonication groups
Group 1 & 2
Sparse Sonication Groups
Group 3 & 5
Dense Sonication groups
Group 4
Very Sparse Sonication Groups
Group 6
Harvesting of Group 1, 3, 4 and 6
Harvesting of Group 2, 5
Blood collection at D0 (before and after sonication), D7-8, D14-15 and D21-22
ELISA quantification of S100β
Postmortem brain collection
B
Control Group 1
Sparse Sonication Group 3
Dense Sonication Group 4
Very Sparse Sonication Group 6
Control group 2
Sparse Sonication Group 5
Animal Weight (in g)
Day 0
Day 7
Day 14
Day 21
Day 28
Day 35
Day 42
Day 84
Weight measurement timeline
C
Control Group 1&2
Sparse Sonication Group 3
Dense Sonication Group 4
Very Sparse Sonication Group 6
Blood concentration of S100β (in pg/mL)
Pre sonication
Post sonication
8d
15d
22d
Post mortem
Days post BBB opening
D
Control Group 1&2
Sparse Sonication Group 5
Blood concentration of S100β (in pg/mL)
Pre sonication
Post sonication
8d
15d
22d
Post mortem
Days post BBB opening

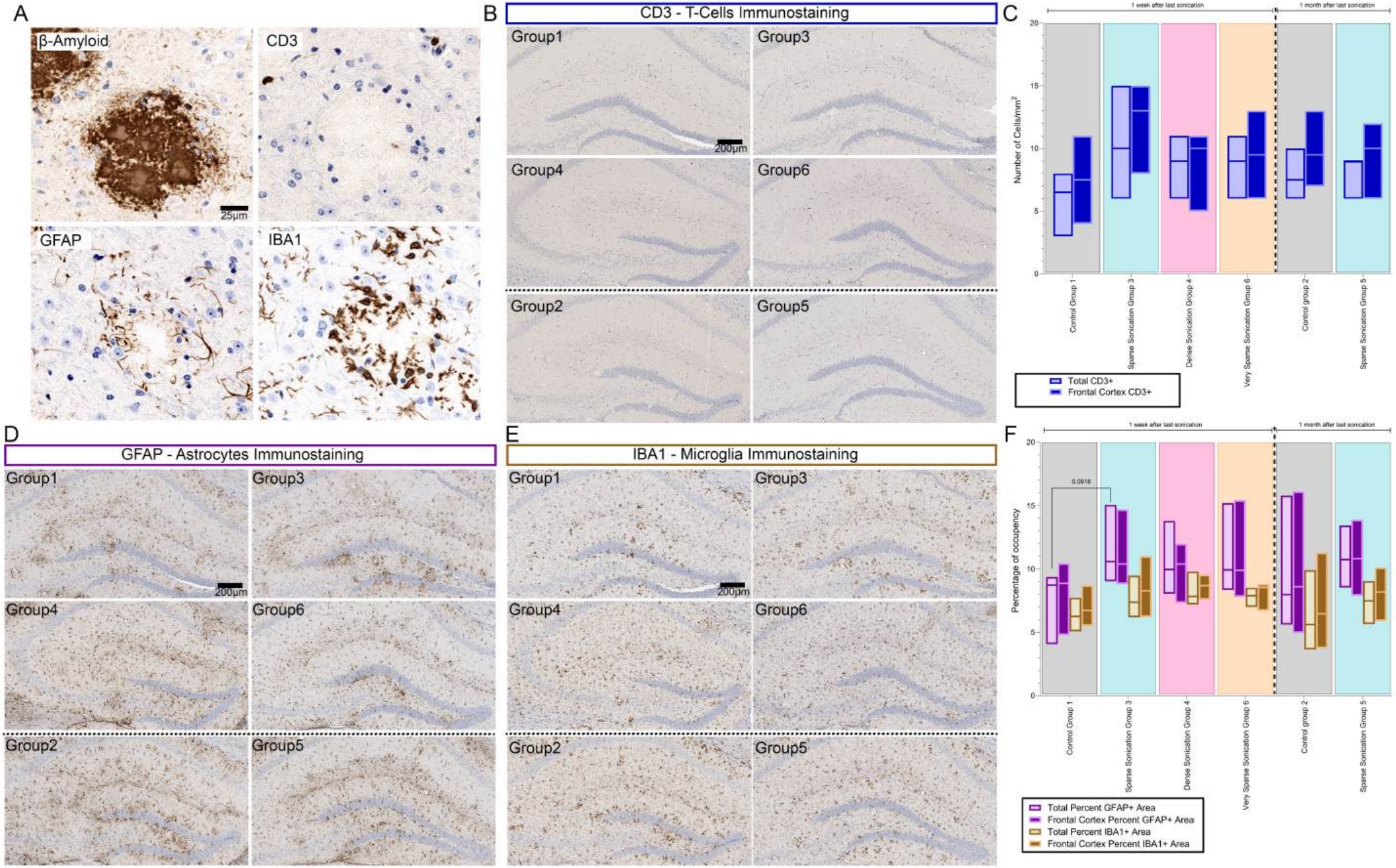
A
β-Amyloid
CD3
25μm
GFAP
IBA1
B
CD3 - T-Cells Immunostaining
Group1
Group3
200μm
Group4
Group6
Group2
Group5
C
1 week after last sonication
1 month after last sonication
Number of Cells/mm²
Control Group 1
Sparse Sonication Group 3
Dense Sonication Group 4
Very Sparse Sonication Group 6
Control group 2
Sparse Sonication Group 5
Total CD3+
Frontal Cortex CD3+
D
GFAP - Astrocytes Immunostaining
Group1
Group3
200μm
Group4
Group6
Group2
Group5
E
IBA1 - Microglia Immunostaining
Group1
Group3
200μm
Group4
Group6
Group2
Group5
F
1 week after last sonication
1 month after last sonication
0.0918
Percentage of occupency
Control Group 1
Sparse Sonication Group 3
Dense Sonication Group 4
Very Sparse Sonication Group 6
Control group 2
Sparse Sonication Group 5
Total Percent GFAP+ Area
Frontal Cortex Percent GFAP+ Area
Total Percent IBA1+ Area
Frontal Cortex Percent IBA1+ Area

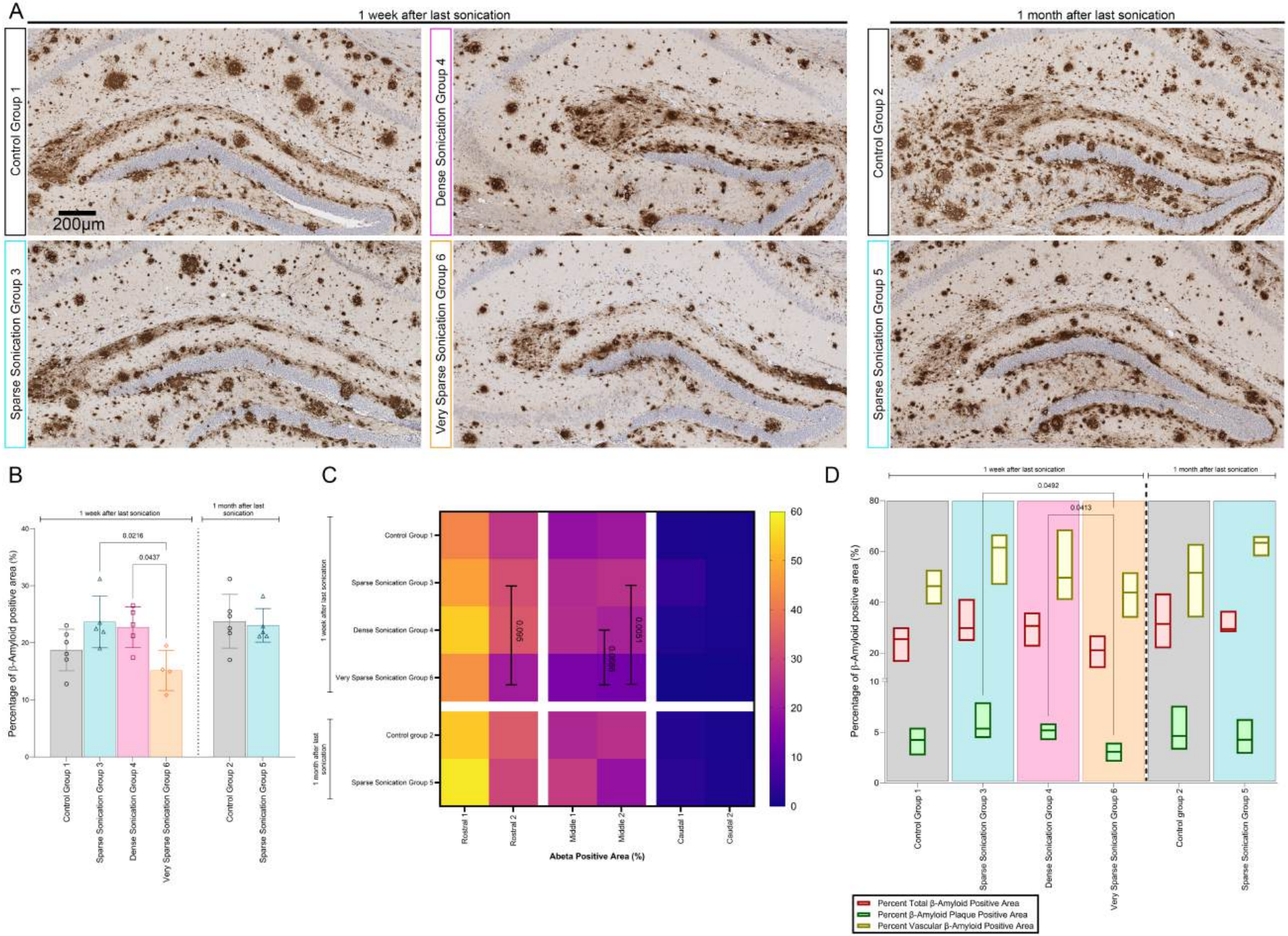
A
1 week after last sonication
1 month after last sonication
Control Group 1
Dense Sonication Group 4
Control Group 2
Sparse Sonication Group 3
Very Sparse Sonication Group 6
Sparse Sonication Group 5
200µm
B
1 week after last sonication
1 month after last sonication
0.0216
0.0437
Percentage of β-Amyloid positive area (%)
Control Group 1
Sparse Sonication Group 3
Dense Sonication Group 4
Very Sparse Sonication Group 6
Control Group 2
Sparse Sonication Group 5
C
Control Group 1
Sparse Sonication Group 3
Dense Sonication Group 4
Very Sparse Sonication Group 6
Control group 2
Sparse Sonication Group 5
1 week after last sonication
1 month after last sonication
Rostral 1
Rostral 2
Middle 1
Middle 2
Caudal 1
Caudal 2
Abeta Positive Area (%)
D
1 week after last sonication
1 month after last sonication
0.0492
0.0413
Percentage of β-Amyloid positive area (%)
Control Group 1
Sparse Sonication Group 3
Dense Sonication Group 4
Very Sparse Sonication Group 6
Control group 2
Sparse Sonication Group 5
Percent Total β-Amyloid Positive Area
Percent β-Amyloid Plaque Positive Area
Percent Vascular β-Amyloid Positive Area

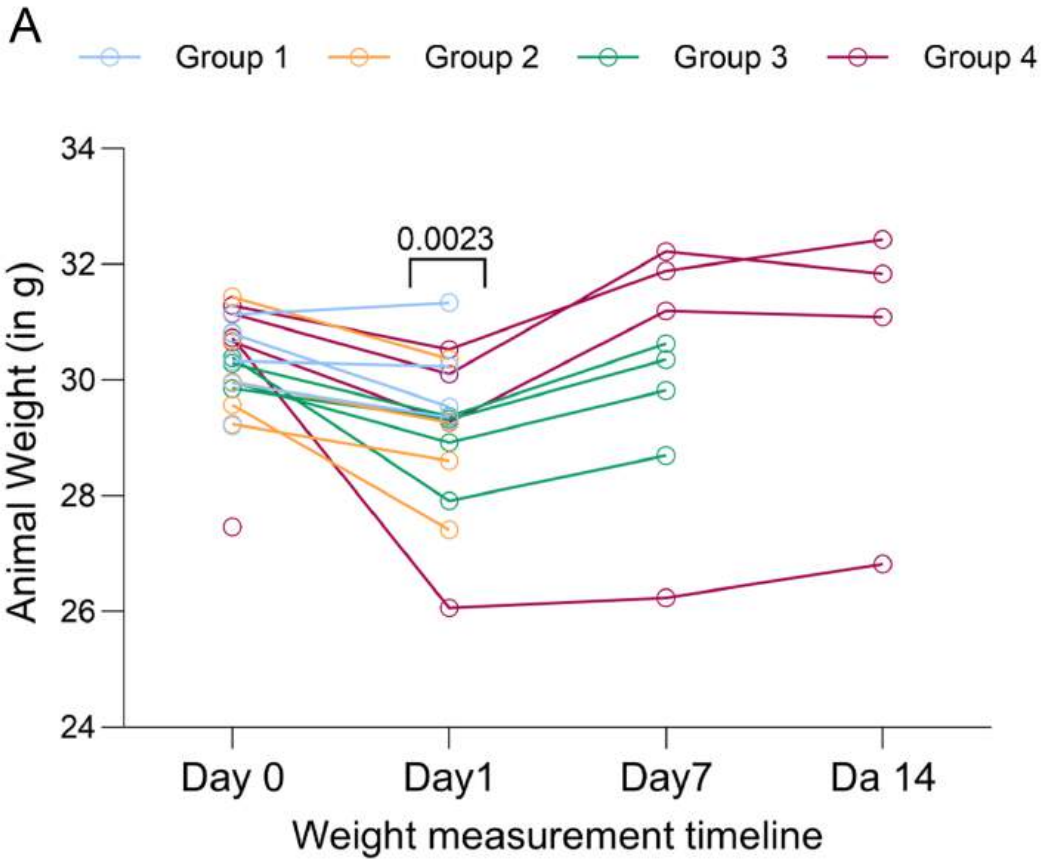
A
Group 1
Group 2
Group 3
Group 4
0.0023
Animal Weight (in g)
34
32
30
28
26
24
Day 0
Day1
Day7
Da 14
Weight measurement timeline

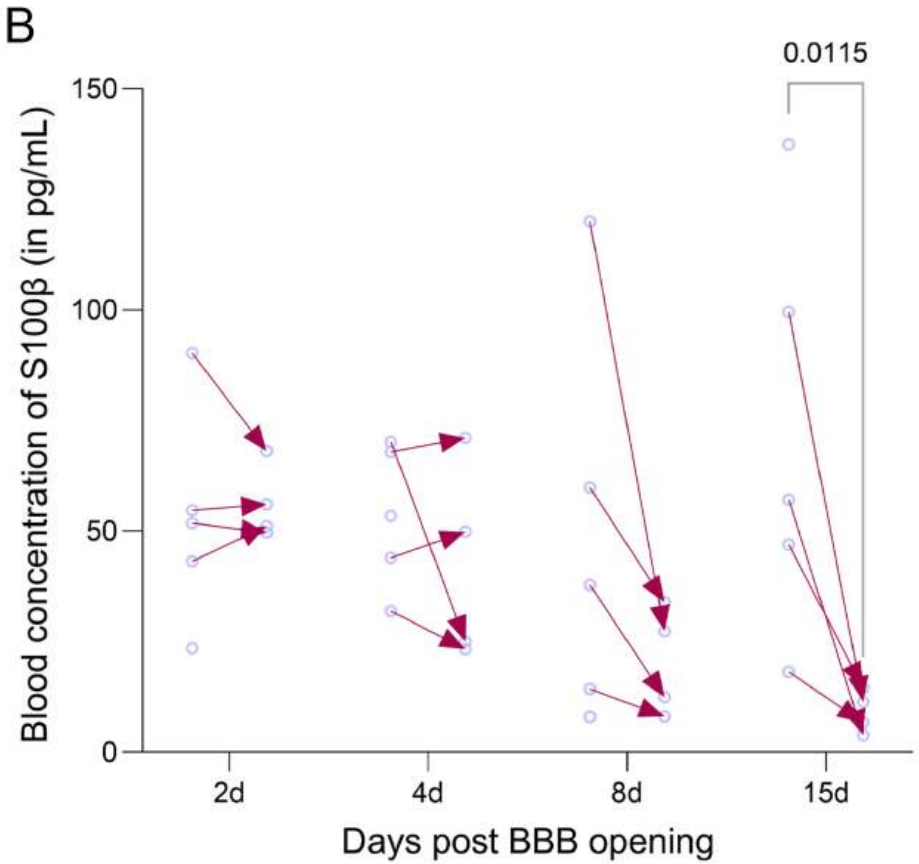
B
0.0115
Blood concentration of S100β (in pg/mL)
150
100
50
0
2d
4d
8d
15d
Days post BBB opening

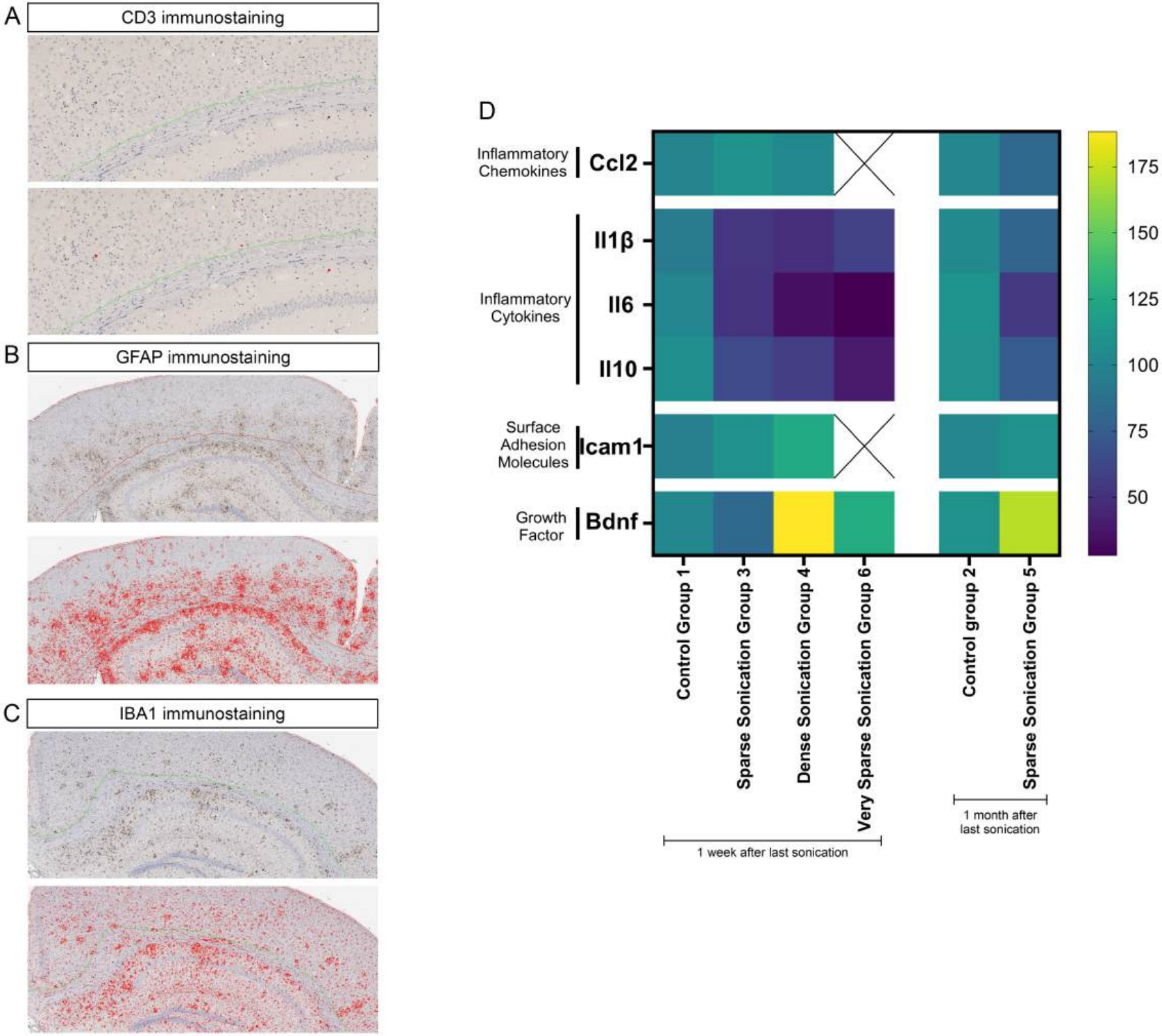
A
CD3 immunostaining
B
GFAP immunostaining
C
IBA1 immunostaining
D
Inflammatory Chemokines
Ccl2
Inflammatory Cytokines
Il1β
Il6
Il10
Surface Adhesion Molecules
Icam1
Growth Factor
Bdnf
Control Group 1
Sparse Sonication Group 3
Dense Sonication Group 4
Very Sparse Sonication Group 6
Control group 2
Sparse Sonication Group 5
1 week after last sonication
1 month after last sonication
175
150
125
100
75
50

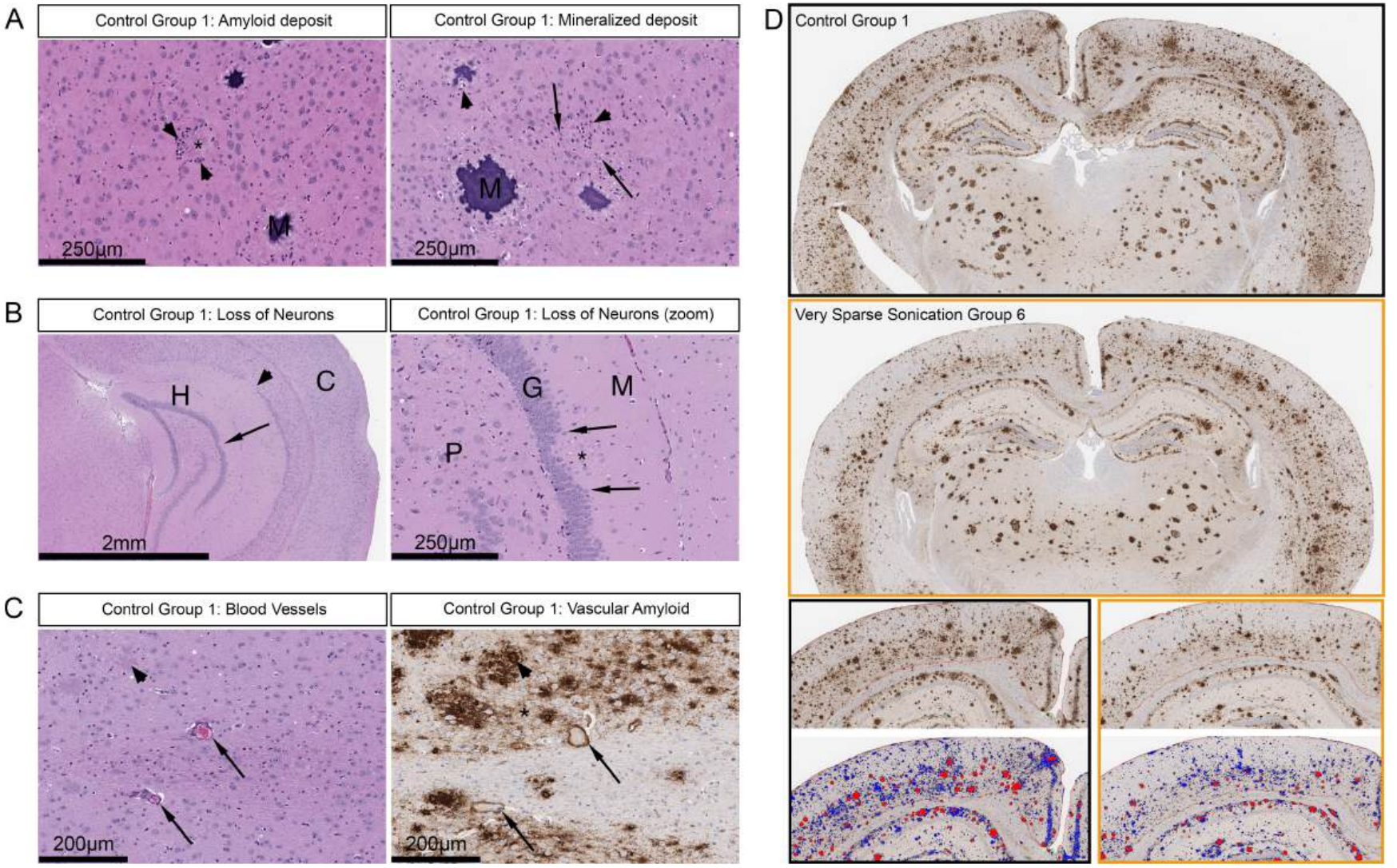
A
Control Group 1: Amyloid deposit
Control Group 1: Mineralized deposit
M
M
250µm
250µm
B
Control Group 1: Loss of Neurons
Control Group 1: Loss of Neurons (zoom)
H
C
G
M
P
2mm
250µm
C
Control Group 1: Blood Vessels
Control Group 1: Vascular Amyloid
200µm
200µm
D
Control Group 1
Very Sparse Sonication Group 6
Total
Frontal Cortex
Number of deposits (per mm²)
Percentage of β-Amyloid deposit area (%)
Total deposit area distribution (in µm²)
0.115429
0.038476
Group1
Group6

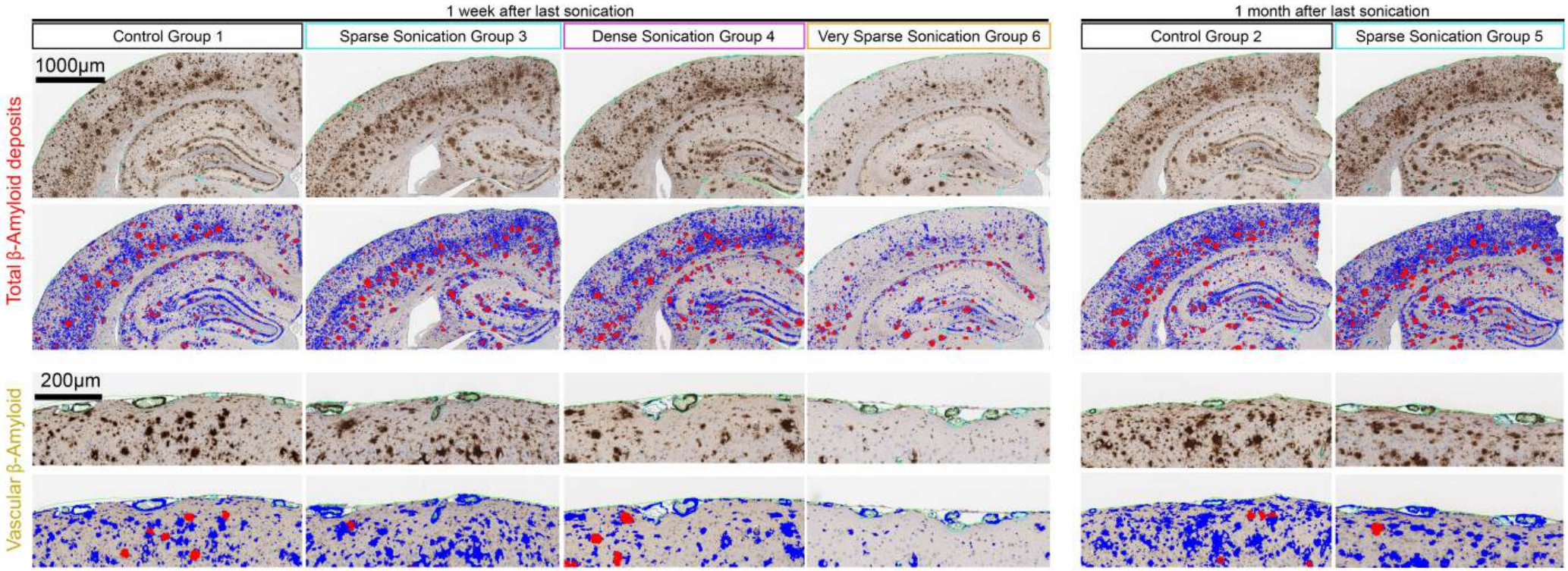
1 week after last sonication
1 month after last sonication
Control Group 1
Sparse Sonication Group 3
Dense Sonication Group 4
Very Sparse Sonication Group 6
Control Group 2
Sparse Sonication Group 5
1000μm
200μm
Total β-Amyloid deposits
Vascular β-Amyloid

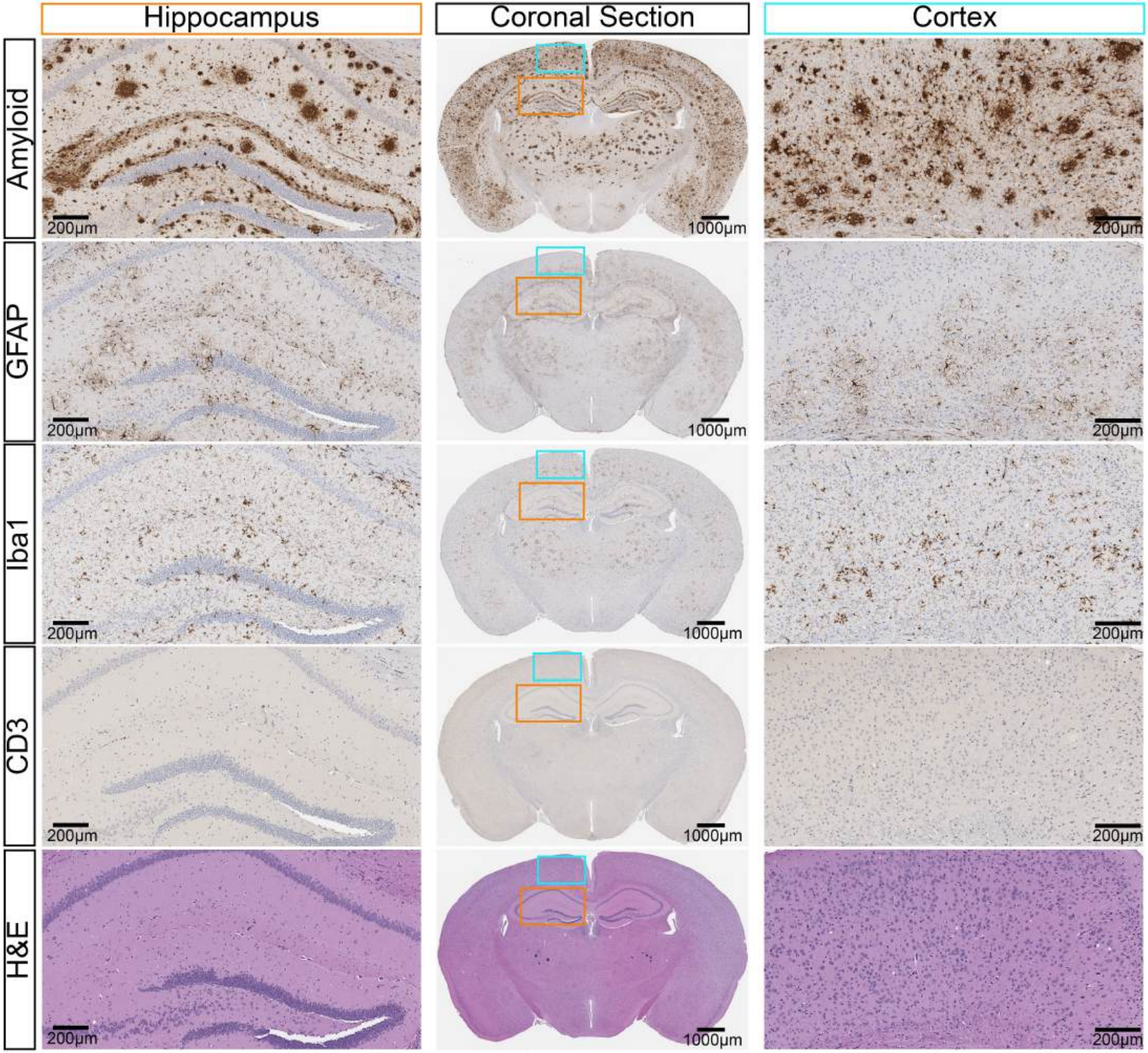
Hippocampus
Coronal Section
Cortex
Amyloid
GFAP
Iba1
CD3
H&E
200μm
1000μm

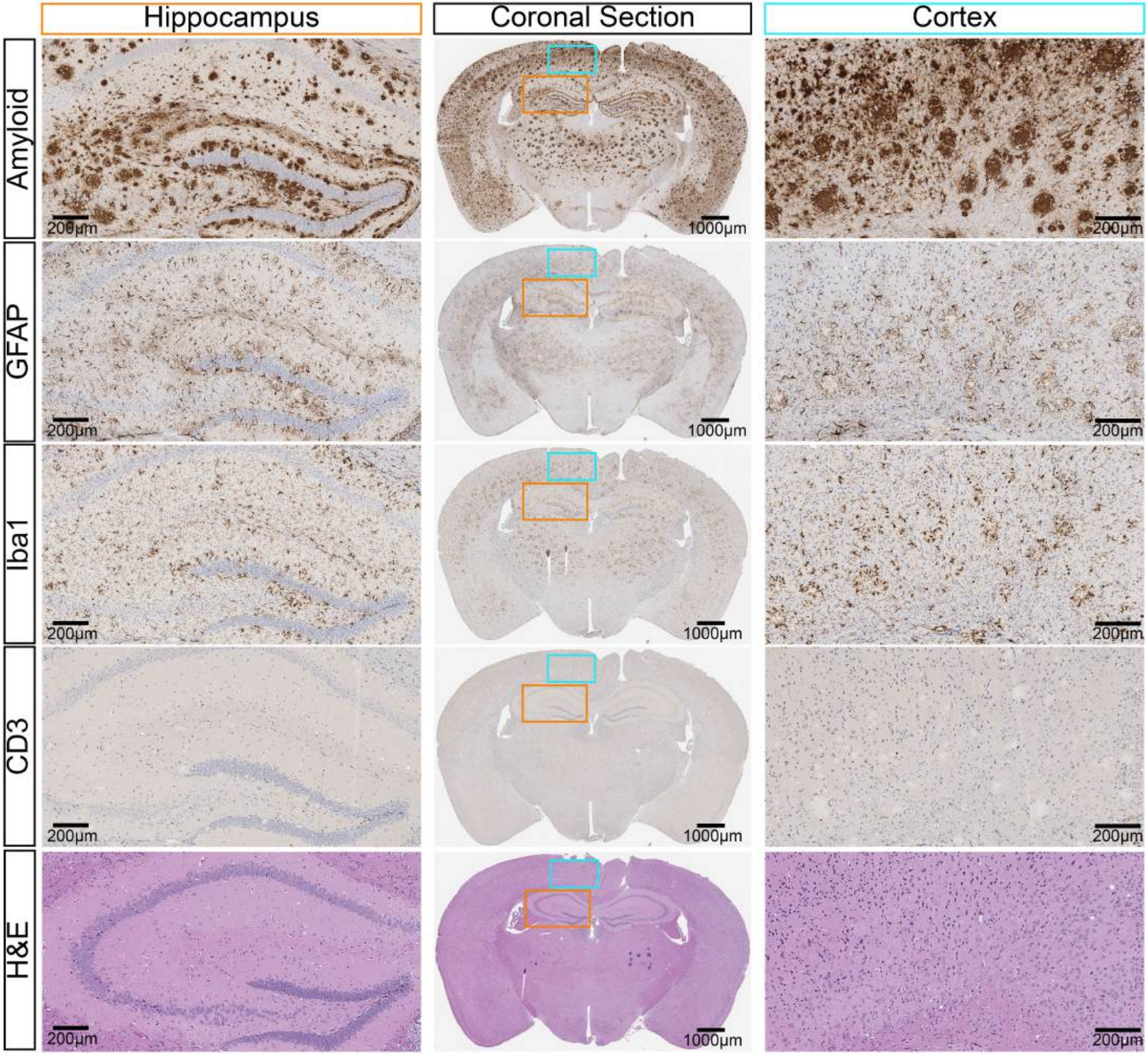
Hippocampus
Coronal Section
Cortex
Amyloid
GFAP
Iba1
CD3
H&E
200μm
1000μm

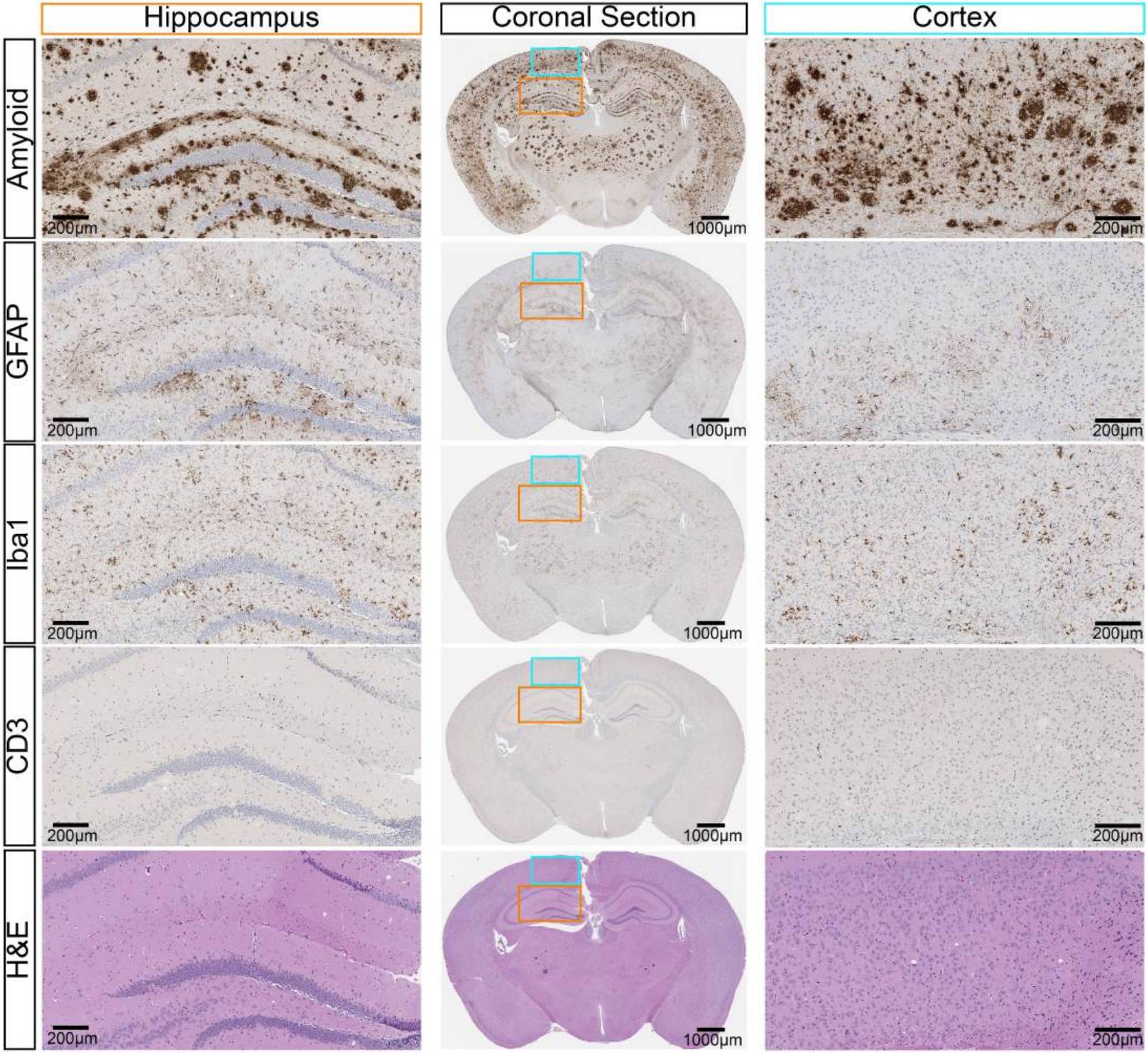
Hippocampus
Coronal Section
Cortex
Amyloid
GFAP
Iba1
CD3
H&E
200μm
1000μm

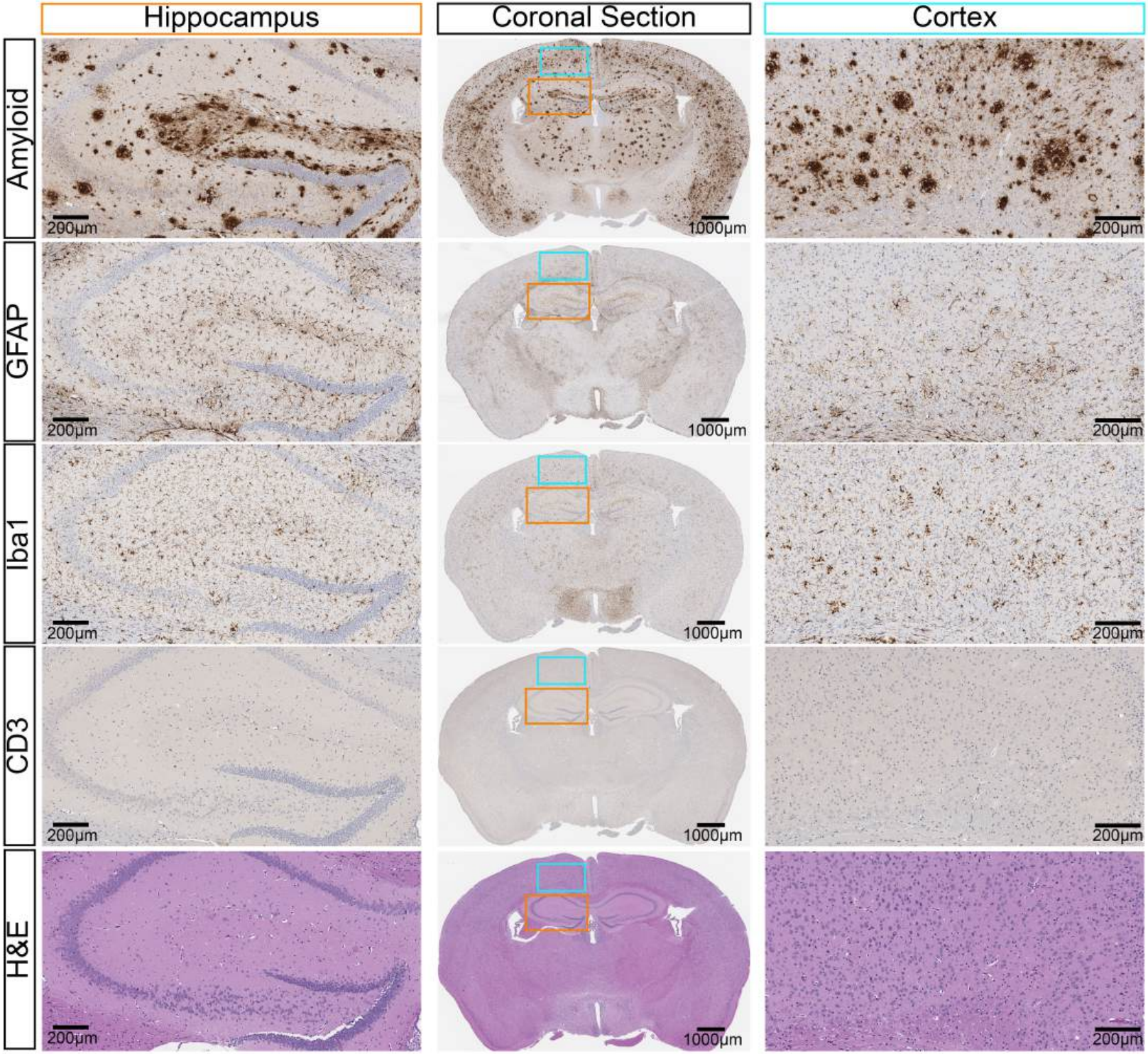
Hippocampus
Coronal Section
Cortex
Amyloid
GFAP
Iba1
CD3
H&E
200μm
1000μm

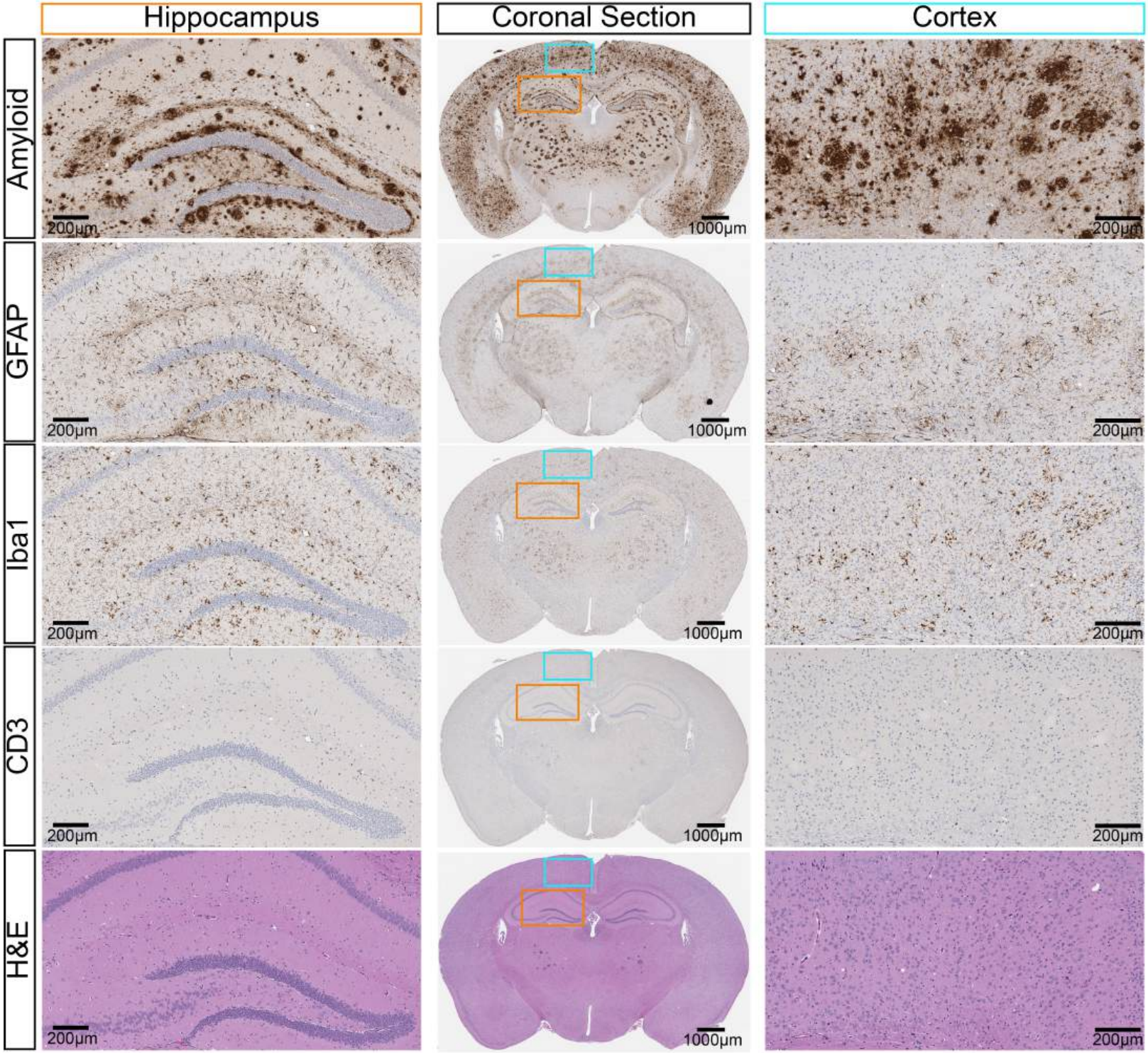
Hippocampus
Coronal Section
Cortex
Amyloid
GFAP
Iba1
CD3
H&E
200μm
1000μm

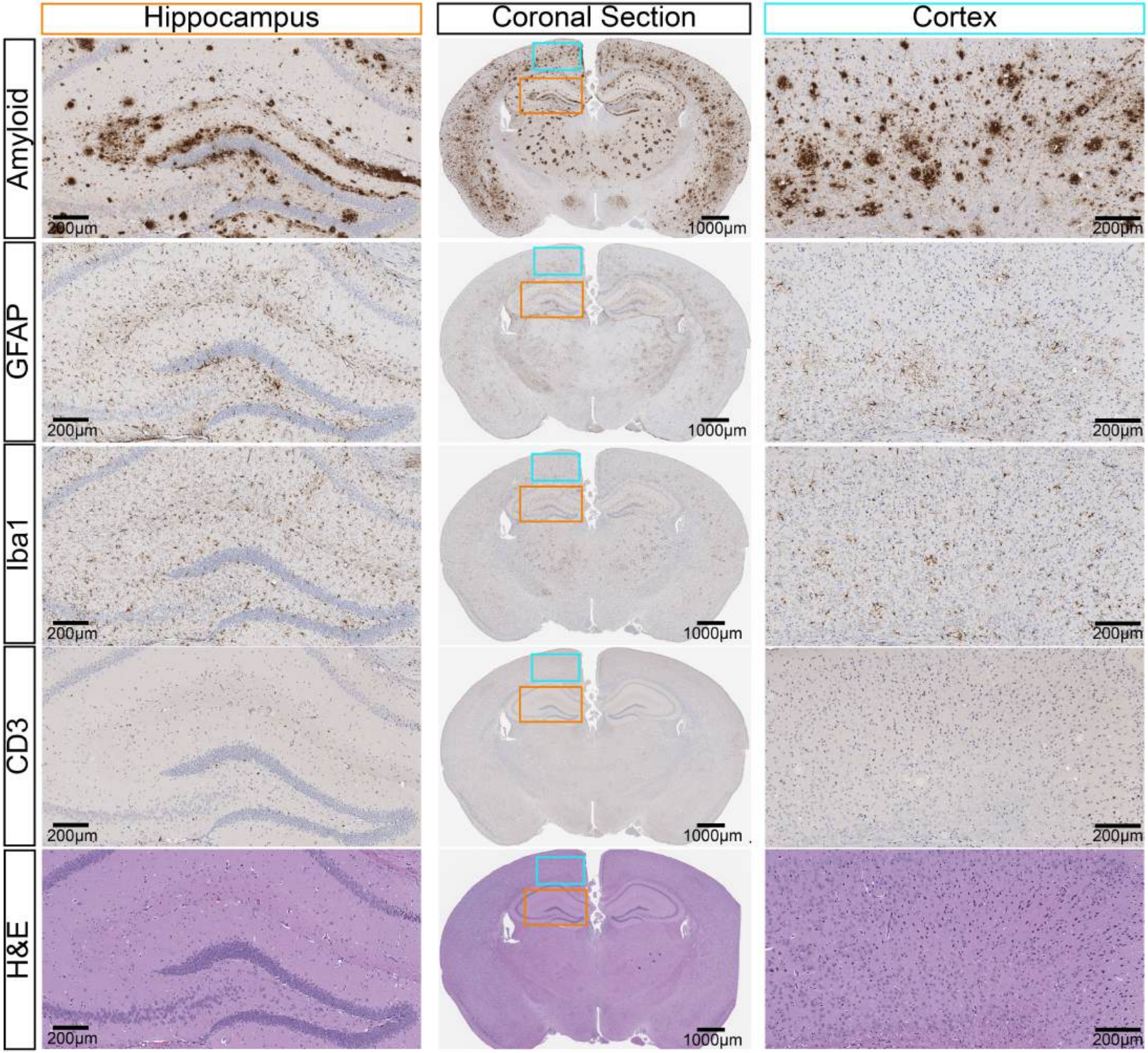
Hippocampus
Coronal Section
Cortex
Amyloid
GFAP
Iba1
CD3
H&E
200μm
1000μm

	Cxcl1			Ccl2			Il1β			Il6			Il10			Tnfα		
	Mean	SD	N	Mean	SD	N	Mean	SD	N	Mean	SD	N	Mean	SD	N	Mean	SD	N
No BBB opening	99.9999999	6.39638142	7	99.9999999	3.30325326	7	100	3.31684234	7	100	2.21083873	7	100	3.18333499	6	100	4.48916116	7
2d post BBB opening	84.1701903	10.3300847	4	85.6161992	1.64140685	4	86.7289878	3.47666786	4	111.936937	3.37861543	4	87.399131	7.02388338	4	91.7602996	2.72942346	4
4d post BBB opening	97.4483204	6.56072308	4	84.1702549	12.1639782	4	78.9595572	9.26497926	4	105.457855	4.13181313	4	82.3091248	6.81195551	3	88.21005	8.0498684	4
8d post BBB opening	89.3910031	5.07905368	4	87.3472594	2.49080473	4	83.644939	3.23633328	4	107.984697	3.04039091	4	90.5234844	1.38846255	3	93.8540366	2.48773547	4
15d post BBB opening	86.4928354	15.2681285	4	85.6976609	1.47683189	4	85.7602802	3.27355627	4	111.461805	1.61981849	4	94.1858059	0.41330404	3	92.5977944	3.56796066	4

	Icam1			E-selectin			Tgfβ			Bdnf			Nfkb1		
	Mean	SD	N	Mean	SD	N	Mean	SD	N	Mean	SD	N	Mean	SD	N
No BBB opening	100	4.98481868	7	100	4.3340069	7	100	2.96480229	7	100	5.51132486	7	100	16.2264476	7
2d post BBB opening	64.494044	8.9441538	4	71.9571264	10.3749887	4	59.3623128	8.09670815	4	73.480663	11.9242656	4	67.6649466	12.1936331	4
4d post BBB opening	72.1662778	4.4780801	4	81.2168297	5.42643355	3	69.5786084	5.15336776	4	90.0636196	6.90450951	4	80.9743212	7.56250881	3
8d post BBB opening	75.8412134	3.1642435	4	87.3489353	5.27094089	4	69.2846143	6.4246666	4	83.0026788	7.85192778	4	76.69554	6.88676532	4
15d post BBB opening	75.5403414	2.01769987	4	84.0422981	9.53785609	4	65.4136917	1.61721509	4	75.7366483	3.326295	4	72.6962772	1.64031966	4

	CCl2			IL-1b			IL-6			TNF			ICAM1			Bdnf1		
	Mean	SD	N	Mean	SD	N	Mean	SD	N	Mean	SD	N	Mean	SD	N	Mean	SD	N
Control Group 1	100	5.64080851	4	100	23.7174991	9	100	15.1470505	7	100	21.8173811	17	100	8.05468398	15	100	8.81438848	18
Sparse Sonication Group 3	105.928533	11.7733734	4	47.8831499	21.7464705	7	49.7764048	9.02670181	6	61.5928659	20.0734448	12	106.820794	20.358028	12	109.067975	62.3874537	15
Dense Sonication Group 4	107.146724	17.2155197	4	48.0101609	24.9578515	13	38.9232127	26.2442241	13	55.6141276	19.1764132	14	128.623785	9.59131353	11	187.925718	20.7368079	15
Very Sparse Sonication Group 6				54.5088907	33.2651908	6	27.9876435	17.2127141	2	46.1715867	23.6504337	8				118.01857	48.1988862	12
Control group 2	100	8.40236401	10	99.9999999	20.9397726	9	100	21.4582402	8	100	19.975462	18	100	10.631707	18	100	26.8140186	13
Sparse Sonication Group 5	83.537182	4.02692703	3	84.0437464	16.0663535	6	61.907884	23.5723261	8	69.7287926	16.8768758	14	103.320948	13.6820944	7	167.101224	21.7228397	15

	Rostral 1			Rostral 2			Middle 1			Middle 2			Caudal 1			Caudal 2		
	Mean	SD	N	Mean	SD	N	Mean	SD	N	Mean	SD	N	Mean	SD	N	Mean	SD	N
Control Group 1	45.0633333	8.84636347	6	26.4366667	5.52090089	6	18.72	4.97570899	6	20.235	5.27793804	6	1.53666667	0.94167227	6	1.08666667	0.80988065	6
Sparse Sonication Group 3	51.554	8.37815194	5	32.4	5.06450886	5	25.356	6.96379422	5	25.132	2.81310682	5	3.19	1.59284337	5	1.252	0.37432606	5
Dense Sonication Group 4	52.242	5.79775991	5	31.006	8.54236091	5	24.794	2.25200577	5	22.134	4.6122424	5	1.708	0.53895269	5	1.134	0.45429066	5
Very Sparse Sonication Group 6	43.505	6.25032532	4	20.665	5.3789807	4	15.905	5.51050209	4	13.1075	2.96266068	4	1.235	1.42348165	4	0.7475	0.38836194	4
Control group 2	52.1633333	8.39945157	6	34.6483333	3.78678448	6	23.5783333	6.79734482	6	25.915	4.65206513	6	2.49833333	1.73152438	6	0.985	0.54309299	6
Sparse Sonication Group 5	57.806	6.49661681	5	30.46	5.54458745	5	27.006	3.18426287	5	19.918	4.69592057	5	2.856	0.92829413	5	1.406	0.28866936	5

Table 4: List of the previous mouse models used in combination with Ultrasound. Four models have been used to explore the effect of sonication on the amyloid pathology:

Mouse model	Strain characteristics	Pathological hallmarks	Publications
3TG model	Mix model for amyloid and tau pathologies Single mutations in APP, MAPT, PSEN2	• Cognitive impairment at 4 months, • LTP deficits at 6 months, • Amyloid deposition after 6 months, • Tau pathology after 1 year	Karakatsani et al., 2023; Noel et al., 2023; Shen et al., 2020; TauPS2APP | ALZFORUM, n.d.
TgCRND8 model	Pure amyloid model Double mutation in APP	• Amyloid deposition at 3 months • Associated with cognitive decline • Changes in LTP at 6 months	Burgess, Dubey, et al., 2014; Burgess, Nhan, et al., 2014; Jordão et al., 2010, 2013; Poon et al., 2017; TgCRND8 | ALZFORUM, n.d.
5xFAD model	Pure amyloid model Triple mutation inAPP and double mutation in PSEN1	• Early amyloid deposition around 2 months • Synaptic loss after 4 months • Associated with cognitive impairments • Changes in LTP and neuronal loss at 6 months	*5xFAD (B6SJL) | ALZFORUM, n.d.; Bobola et al., 2020; Lee et al., 2020*
APP/PS1dE9 model	Pure amyloid model Single mutations in APP and PSEN1	• Early LTP impairment at 3 months • Synaptic loss at 4 months • Amyloid deposition at 6 months • Cognitive impairment around 1 year	*APPswe/PSEN1dE9 (C57BL6) | ALZFORUM*, n.d.; Hsu et al., 2018; Sun et al., 2021

5xFAD (B6SJL) | ALZFORUM. (n.d.). Retrieved 27 November 2024, from https://www.alzforum.org/research-models/5xfad-b6sjl

APPswe/PSEN1dE9 (C57BL6) | ALZFORUM. (n.d.). Retrieved 27 November 2024, from https://www.alzforum.org/research-models/appswepsen1de9-c57bl6

Bobola, M. S., Chen, L., Ezeokeke, C. K., Olmstead, T. A., Nguyen, C., Sahota, A., Williams, R. G., & Mourad, P. D. (2020). Transcranial focused ultrasound, pulsed at 40 Hz, activates microglia acutely and reduces Aβ load chronically, as demonstrated in vivo. *Brain Stimulation*, *13*(4), 1014–1023. https://doi.org/10.1016/J.BRS.2020.03.016

Burgess, A., Dubey, S., Yeung, S., Hough, O., Eterman, N., Aubert, I., & Hynynen, K. (2014). Alzheimer Disease in a Mouse Model: MR Imaging–guided Focused Ultrasound Targeted to the Hippocampus Opens the Blood-Brain Barrier and Improves Pathologic Abnormalities and Behavior. *Https://Doi.Org/10.1148/Radiol.14140245*, *273*(3), 736–745. https://doi.org/10.1148/RADIOL.14140245

Burgess, A., Nhan, T., Moffatt, C., Klibanov, A. L., & Hynynen, K. (2014). Analysis of focused ultrasound-induced blood-brain barrier permeability in a mouse model of Alzheimer's disease using two-photon microscopy. *Journal of Controlled Release*, *192*, 243–248. https://doi.org/10.1016/j.jconrel.2014.07.051

Hsu, P. H., Lin, Y. T., Chung, Y. H., Lin, K. J., Yang, L. Y., Yen, T. C., & Liu, H. L. (2018). Focused Ultrasound-Induced Blood-Brain Barrier Opening Enhances GSK-3 Inhibitor Delivery for Amyloid-Beta Plaque Reduction. *Scientific Reports 2018 8:1*, *8*(1), 1–9. https://doi.org/10.1038/s41598-018-31071-8

Jordão, J. F., Ayala-Grosso, C. A., Markham, K., Huang, Y., Chopra, R., McLaurin, J. A., Hynynen, K., & Aubert, I. (2010). Antibodies Targeted to the Brain with Image-Guided Focused Ultrasound Reduces Amyloid-β Plaque Load in the TgCRND8 Mouse Model of Alzheimer's Disease. *PLOS ONE*, *5*(5), e10549. https://doi.org/10.1371/JOURNAL.PONE.0010549

Jordão, J. F., Thévenot, E., Markham-Coultes, K., Scarcelli, T., Weng, Y. Q., Xhima, K., O'Reilly, M., Huang, Y., McLaurin, J. A., Hynynen, K., & Aubert, I. (2013). Amyloid-β plaque reduction, endogenous antibody delivery and glial activation by brain-targeted, transcranial focused ultrasound. *Experimental Neurology*, *248*, 16–29. https://doi.org/10.1016/J.EXPNEUROL.2013.05.008

Karakatsani, M. E., Ji, R., Murillo, M. F., Kugelman, T., Kwon, N., Lao, Y. H., Liu, K., Pouliopoulos, A. N., Honig, L. S., Duff, K. E., & Konofagou, E. E. (2023). Focused ultrasound mitigates pathology and improves spatial memory in Alzheimer's mice and patients. *Theranostics*, *13*(12), 4102–4120. https://doi.org/10.7150/THNO.79898

Lee, Y., Choi, Y., Park, E. J., Kwon, S., Kim, H., Lee, J. Y., & Lee, D. S. (2020). Improvement of glymphatic-lymphatic drainage of beta-amyloid by focused ultrasound in Alzheimer's disease model. *Scientific Reports*, *10*(1). https://doi.org/10.1038/S41598-020-73151-8

Noel, R. L., Gorman, S. L., Batts, A. J., & Konofagou, E. E. (2023). Getting ahead of Alzheimer's disease: early intervention with focused ultrasound. *Frontiers in Neuroscience*, *17*. https://doi.org/10.3389/FNINS.2023.1229683

Poon, C., McMahon, D., & Hynynen, K. (2017). Noninvasive and targeted delivery of therapeutics to the brain using focused ultrasound. *Neuropharmacology*, *120*, 20–37.

Shen, Y., Hua, L., Yeh, C. K., Shen, L., Ying, M., Zhang, Z., Liu, G., Li, S., Chen, S., Chen, X., & Yang, X. (2020). Ultrasound with microbubbles improves memory, ameliorates pathology and modulates hippocampal proteomic changes in a triple transgenic mouse model of Alzheimer's disease. *Theranostics*, *10*(25), 11794–11819. https://doi.org/10.7150/THNO.44152

Sun, T., Shi, Q., Zhang, Y., Power, C., Hoesch, C., Antonelli, S., Schroeder, M. K., Caldarone, B. J., Taudte, N., Schenk, M., Hettmann, T., Schilling, S., McDannold, N. J., & Lemere, C. A. (2021). Focused ultrasound with anti-pGlu3 Aβ enhances efficacy in Alzheimer's disease-like mice via recruitment of peripheral immune cells. *Journal of Controlled Release : Official Journal of the Controlled Release Society*, *336*, 443–456. https://doi.org/10.1016/J.JCONREL.2021.06.037

TauPS2APP | ALZFORUM. (n.d.). Retrieved 27 November 2024, from https://www.alzforum.org/research-models/taups2app

TgCRND8 | ALZFORUM. (n.d.). Retrieved 27 November 2024, from https://www.alzforum.org/research-models/tgcrnd8

Study	Model used	Age of the model	Sonication treatment	Associated therapeutics	Effect on the pathology	Effect on behavior
Shen et al, 2020[1]	3TG	8 mo	Repeated, twice a week for six weeks	none	• Decreased amyloid burden in Cortex, CA and amygdala • Reduced Tau phosphorylation • Reduced branching and process length in microglia • Axonal protection	Improvement in Y maze, Morris water maze and step down avoidance test
Noel et al, 2023[2]	3TG	2.5mo 1 yo 2 yo	One treatment	none	Opening volume slightly higher in 3TG compared to WT	NA
Karakatsani et al, 2023[3]	3TG	14 mo	Repeated, once a week for four weeks	none	>50% reduction in number and 42% in size	Improvement of memory (Morris water maze)
Jordao et al, 2013[4]	TgCRND8	4 mo	One treatment	none	• Reduced deposits in cortex • IgG & IgM to penetrate infiltration • Increased in Iba1 and GFAP • Increased distal localization of microglia and astrocytes • Increased neuronal area • Increased colocalization between glial cells and amyloid deposits	NA
Burgess et al, 2014a[5]	TgCRND8	7 mo	Repeated, once a week for 3 weeks, bilateral	none	• Decreased in deposit size (~20%) and deposit number (~19%) • Increased in DCX positive neurons (188% for nTG, 252% for Tg) • Increased in dendrite length and branching	Improvement at the Y maze
Burgess et al, 2014b[6]	TgCRND8	6-8 mo	One treatment	none	• Correlation of vessel diameter and leakage probability • Vessels displaying leakage are significantly smaller in Tg mice • Vessels coated with amyloid show less changes in diameter	NA
Poon et al, 2017[7]	TgCRND8	7 mo	Repeated, once a week for 5 weeks	none	• Decreased number of amyloid deposits • Decrease amyloid deposit area	NA
Bobola et al, 2020[8]	5xFAD	6 mo	Repeated, daily for five days	none	• Decreased amyloid burden by ~50% compared to control	NA

					• Increased microglia colocalization with amyloid deposits compared to control	
Lee et al, 2020[9]	5xFAD	4 mo	Repeated, once a week for six weeks	none	• Decrease of both amyloid deposits area and deposit area • Increased CSF abeta	Improvement in working memory
Jordao et al, 2010[10]	TgCRND8	4.5 mo	One treatment	BAM10 antibody	Slight decrease in Abeta deposits	NA
Alecou et al, 2017[11]	Rabbit, high cholesterol diet	Not disclosed	Repeated, three treatments	BC-10 (sigma), anti Amyloid-beta antibody	Original amyloid deposit density 200/cm2, decreased to 78/cm2 after treatment	NA
Hsu et al, 2018[12]	APP/PS1dE9	12-14 mo	Repeated, once a week for five weeks	GSK-3 Inhibitor	Significant decrease of the deposit size in hippocampus, including with FUS alone	NA
Sun et al, 2021[13]	APP/PS1dE9	16 mo, 24-30 mo	Three treatments for 16mo cohort, one treatment for 24-30mo cohort	anti-pGlu3 (07/2a)	• Decreased hippocampal plaque deposition in APP/PS1dE9 mice co-treated with anti-pGlu3 Aβ mAb and FUS-BBBD • Age-related hippocampal synaptic degeneration is reduced in APP/PS1dE9 mice after treatment with 07/2a and FUS-BBBD • Altered plaque-associated microglia and macrophage activation in aged APP/PS1dE9 after treatment with 07/2a and FUS-BBBD	No significant effects in fear learning and memory or locomotor activity with anti-pGlu3 Aβ mAb or FUS-BBBD
Deng et al, 2021[14]	APP/PS1dE9	10 mo	One treatment	IV injection of US-HA-Exo	Decreased deposit area and occupancy	NA
Antoniou et al, 2024[15]	5xFAD	5 mo	One treatment	Amyloid Protein (1–40) antibody produced in rabbit whole antiserum, A8326	Allow for non-invasive antibody delivery to amyloid deposits	NA

Table 5: Previous studies using ultrasound in mouse models for Alzheimer's Disease and their output.

1. Shen, Y., Hua, L., Yeh, C. K., Shen, L., Ying, M., Zhang, Z., Liu, G., Li, S., Chen, S., Chen, X. & Yang, X. Ultrasound with microbubbles improves memory, ameliorates pathology and modulates hippocampal proteomic changes in a triple transgenic mouse model of Alzheimer's disease. *Theranostics* 10, 11794–11819 (2020).

2. Noel, R. L., Gorman, S. L., Batts, A. J. & Konofagou, E. E. Getting ahead of Alzheimer's disease: early intervention with focused ultrasound. *Front Neurosci* 17, (2023).

3. Karakatsani, M. E., Ji, R., Murillo, M. F., Kugelman, T., Kwon, N., Lao, Y. H., Liu, K., Pouliopoulos, A. N., Honig, L. S., Duff, K. E. & Konofagou, E. E. Focused ultrasound mitigates pathology and improves spatial memory in Alzheimer's mice and patients. *Theranostics* 13, 4102–4120 (2023).

4. Jordão, J. F., Thévenot, E., Markham-Coultes, K., Scarcelli, T., Weng, Y. Q., Xhima, K., O'Reilly, M., Huang, Y., McLaurin, J. A., Hynynen, K. & Aubert, I. Amyloid-β plaque reduction, endogenous antibody delivery and glial activation by brain-targeted, transcranial focused ultrasound. *Exp Neurol* 248, 16–29 (2013).

5. Burgess, A., Dubey, S., Yeung, S., Hough, O., Eterman, N., Aubert, I. & Hynynen, K. Alzheimer Disease in a Mouse Model: MR Imaging–guided Focused Ultrasound Targeted to the Hippocampus Opens the Blood-Brain Barrier and Improves Pathologic Abnormalities and Behavior. *https://doi.org/10.1148/radiol.14140245* 273, 736–745 (2014).

6. Burgess, A., Nhan, T., Moffatt, C., Klibanov, A. L. & Hynynen, K. Analysis of focused ultrasound-induced blood-brain barrier permeability in a mouse model of Alzheimer's disease using two-photon microscopy. *Journal of Controlled Release* 192, 243–248 (2014).

7. Poon, C., McMahon, D. & Hynynen, K. Noninvasive and targeted delivery of therapeutics to the brain using focused ultrasound. *Neuropharmacology* 120, 20–37 (2017).

8. Bobola, M. S., Chen, L., Ezeokeke, C. K., Olmstead, T. A., Nguyen, C., Sahota, A., Williams, R. G. & Mourad, P. D. Transcranial focused ultrasound, pulsed at 40 Hz, activates microglia acutely and reduces Aβ load chronically, as demonstrated in vivo. *Brain Stimul* 13, 1014–1023 (2020).

9. Lee, Y., Choi, Y., Park, E. J., Kwon, S., Kim, H., Lee, J. Y. & Lee, D. S. Improvement of glymphatic-lymphatic drainage of beta-amyloid by focused ultrasound in Alzheimer's disease model. *Sci Rep* 10, (2020).

10. Jordão, J. F., Ayala-Grosso, C. A., Markham, K., Huang, Y., Chopra, R., McLaurin, J. A., Hynynen, K. & Aubert, I. Antibodies Targeted to the Brain with Image-Guided Focused Ultrasound Reduces Amyloid-β Plaque Load in the TgCRND8 Mouse Model of Alzheimer's Disease. *PLoS One* 5, e10549 (2010).

11. Alecou, T., Giannakou, M. & Damianou, C. Amyloid β Plaque Reduction With Antibodies Crossing the Blood-Brain Barrier, Which Was Opened in 3 Sessions of Focused Ultrasound in a Rabbit Model. *Journal of Ultrasound in Medicine* n/a--n/a (2017). doi:10.1002/jum.14256

12. Hsu, P. H., Lin, Y. T., Chung, Y. H., Lin, K. J., Yang, L. Y., Yen, T. C. & Liu, H. L. Focused Ultrasound-Induced Blood-Brain Barrier Opening Enhances GSK-3 Inhibitor Delivery for Amyloid-Beta Plaque Reduction. *Scientific Reports 2018 8:1* 8, 1–9 (2018).

13. Sun, T., Shi, Q., Zhang, Y., Power, C., Hoesch, C., Antonelli, S., Schroeder, M. K., Caldarone, B. J., Taudte, N., Schenk, M., Hettmann, T., Schilling, S., McDannold, N. J. & Lemere, C. A. Focused ultrasound with anti-pGlu3 Aβ enhances efficacy in Alzheimer's disease-like mice via recruitment of peripheral immune cells. *J Control Release* 336, 443–456 (2021).

14. Deng, Z., Wang, J., Xiao, Y., Li, F., Niu, L., Liu, X., Meng, L. & Zheng, H. Ultrasound-mediated augmented exosome release from astrocytes alleviates amyloid-β-induced neurotoxicity. *Theranostics* 11, 4351–4362 (2021).

15. Antoniou, A., Stavrou, M., Evripidou, N., Georgiou, E., Kousiappa, I., Koupparis, A., Papacostas, S. S., Kleopa, K. A. & Damianou, C. FUS-mediated blood–brain barrier disruption for delivering anti-Aβ antibodies in 5XFAD Alzheimer's disease mice. *J Ultrasound* 27, 251–262 (2024).